
Contents

15 Gamma-ray bursts	<i>page</i> 1
15.1 Introduction	1
15.2 The big picture	2
15.3 Some technical details	3
15.4 The bursting phase	4
15.5 GRB theory - the generic picture	7
15.6 The afterglow: theory	11
15.7 The afterglow revolution	16
15.8 Collimated outflow (jets): theory	18
15.9 Observational evidence for collimated outflow (jets)	21
15.10 Polarization - A promising tool	22
15.11 The Reverse Shock Emission: Theory and Observations	24
15.12 GRB Host Galaxies and Redshifts	27
15.13 GRBs and Cosmology	31
15.14 Acknowledgments	34
References	35

Cosmic Gamma-Ray Bursts, Their Afterglows, and Their Host Galaxies

K. HURLEY
*University of California
Space Sciences Laboratory
Berkeley, CA*

R. SARI
*California Institute of Technology
Theoretical Astrophysics
Pasadena, CA*

S. G. DJORGOVSKI
*California Institute of Technology
Palomar Observatory
Pasadena, CA*

15.1 Introduction

Regarded as an astrophysical mystery and a curiosity for decades, cosmic gamma-ray bursts are finally entering the mainstream of astronomy and astrophysics. In the past five years, we have learned that they lie at cosmological distances, and are probably caused, possibly among other things, by the collapses and subsequent explosions of massive stars. Energetically they are roughly analogous to supernovae, to which they may indeed be related in some cases; no new physics needs to be invented to explain their prodigious luminosities. Unlike supernovae, however, they are relatively rare, and their energy output is distributed quite differently over wavelength and time. They can probably be observed out to distances comparable to, or even farther than, those of the most distant quasars, which makes them useful to cosmologists as lighthouses to the early universe. Finally, too, they hold the promise of revealing properties of early galaxies such as star formation rates and metallicities in ways that are unique. For all of these reasons, in addition to the facts that they signal the formation of black holes and drive ultra-relativistic winds, they have begun to attract the attention of people working in very diverse disciplines. The words “gamma-ray burst” have even begun to enter the vocabulary of the general public, which regards them with a certain morbid fascination.

It was not at all clear a decade ago that the study of gamma-ray bursts (GRBs) had such a promising future. If, as many people then suspected, they were generated by some sort of activity on galactic neutron stars, they would probably not have been observable for more than the 10's of seconds of the bursts themselves, and they might well have remained a curiosity. Two popular accounts of how our understanding of GRBs evolved have now appeared (Katz 2002; Schilling 2002), so in this chapter

2 *Gamma-ray bursts*

we will forego the intriguing history of the subject, and begin by describing the phenomenology of bursts. The brief gamma-ray emitting phase is followed by a longer duration, long-wavelength “afterglow”; the characteristics and the theory of afterglows are described next. Finally, the observations of afterglows often lead to the identification of the host galaxies of bursts, which are treated in the last section of this chapter.

In this rapidly evolving field, some of the most up-to-date information is found on websites. A non-exhaustive list of them is:

The Interplanetary Network: ssl.berkeley.edu/ipn3/index.html

HETE-II: space.mit.edu/HETE

BATSE: www.batse.msfc.nasa.gov/batse/

BeppoSAX: www.asdc.asi.it/bepposax/

Swift: swift.gsfc.nasa.gov

The gamma-ray burst coordinates network: gcn.gsfc.nasa.gov/gcn/

Jochen Greiner’s afterglow website: www.mpe.mpg.de/~jcg/grb.html

A radio catalog of gamma-ray burst afterglows: www.aoc.nrao.edu/~frail/grb_public.html

The most recent conference proceedings is “Gamma-Ray Bursts in the Afterglow Era” , edited by Costa, Frontera, & Hjorth (2001).

15.2 The big picture

A typical GRB occurs in a star-forming region of a galaxy at a redshift $z \approx 1$. In currently popular models, it is caused by the collapse of a massive star (≈ 30 solar masses) which has exhausted its nuclear fuel supply. The star collapses to a black hole threaded by a strong magnetic field, and possibly fed by an accretion torus. In this configuration, energy can be extracted through the Blandford-Znajek (1977) mechanism. This energy goes into accelerating shells of matter, once part of the massive star, to ultra-relativistic velocities (Lorentz factors of several hundred). These shells collide with one another as they move outward, producing “internal” shocks in a solar-system sized volume. The shocks accelerate electrons, and the electrons emit synchrotron radiation. In the observer’s frame, the radiation appears in gamma-rays, and produces a burst with ≈ 20 second duration. If the gamma-rays were emitted isotropically, they would account for well over 10^{53} erg of energy in many cases. However, there is evidence that this gamma-radiation is strongly beamed, within a cone whose opening angle is only several degrees (Frail et al. 2001) and thus that the total energy emitted in this stage is some two orders of magnitude smaller. As the shells continue to move outward, they eventually reach a region of enhanced density. This could be either the interstellar medium, or a region which was populated with matter by the massive star in its final stages of evolution. As the shells impinge on this region, they produce “external” shocks, which give rise to a long-lived radio, optical, and X-ray afterglow which may be detectable for years in the radio, weeks to months in the optical, and weeks in X-rays. There is about an order of magnitude less energy in the afterglow than in the burst itself. Initially, this afterglow radiation is beamed, but as the shells decelerate, they spread laterally and the radiation tends towards isotropy. The afterglow tends to fade as a power law with time. However, in many cases, the decline is not completely monotonic;

“bumps” can appear in the optical lightcurve, and they have been interpreted either as a supernova-like component or as the result of microlensing.

The model described above is known as the “standard fireball model”. Such models had been discussed extensively long before the GRB distance scale was known, but the establishment of a cosmological distance scale for bursts brought them into sharp focus (Wijers, Rees, & Meszaros 1997). To be sure, there are competing models, as well as variations on this theme, and they cannot be ruled out. Afterglows are only detected for about one-half the bursts. In those cases where they are not detected, the host galaxies cannot be identified, and it is almost impossible to demonstrate that the GRB is due to the collapse of a massive star, as opposed to the merger of two neutron stars, for example.

Because the gamma-rays are beamed, we detect only a small fraction of them. The most sensitive GRB detector flown (BATSE aboard the Compton Gamma-Ray Observatory) detected roughly one burst per day down to its threshold, and missed about one per day due to well understood effects such as Earth-blocking. Using current estimates of beaming, this implies that the Universe-wide GRB rate is at least 1000/day, and possibly more if there are many weaker bursts that were not detected by BATSE.

15.3 Some technical details

Before the radio, optical, or X-ray afterglow can be identified, the burst must be localized rapidly (i.e. within a day or so) to reasonable accuracy (several 10's of arcminutes) during the bursting phase, which typically lasts only several 10's of seconds. The two main ways to do this are first, using a coded mask detection system (e.g. BeppoSAX, Costa et al. 1997) and second, by timing the arrival of the burst at spacecraft separated by interplanetary distances (the Interplanetary Network, Hurley et al. 2000). Burst detection rates using these techniques can reach ≈ 0.5 to one per day.

Next, the position of the burst must be communicated rapidly to observers. This is now done almost exclusively through the Gamma-Ray Burst Coordinates Network (GCN, Barthelmy, Cline, & Butterworth 2001), which reaches almost 600 recipients. In the early phases, the afterglow may be bright enough to be detected by amateur astronomers with telescopes of modest size ($m \approx 16$ in the day or so following the burst; in many cases, the burst outshines its host galaxy). This phase is crucial, because the position of an optical afterglow must be determined to arcsecond accuracy or better to allow optical spectroscopy to take place with telescopes of much larger size, as well as to permit deep observations which may reveal the presence of a host galaxy.

In many cases, the X-ray afterglow has been observed within hours of the burst by the same spacecraft which localized the burst, after slewing to the position (BeppoSAX, Costa 2000). In other cases, target-of-opportunity observations have been carried out with a different spacecraft from the one which detected the burst, but with much longer delays.

Radio measurements can be carried out at a more leisurely pace, since the radio emission tends to peak days after the event (Frail, Waxman, & Kulkarni 2000). But

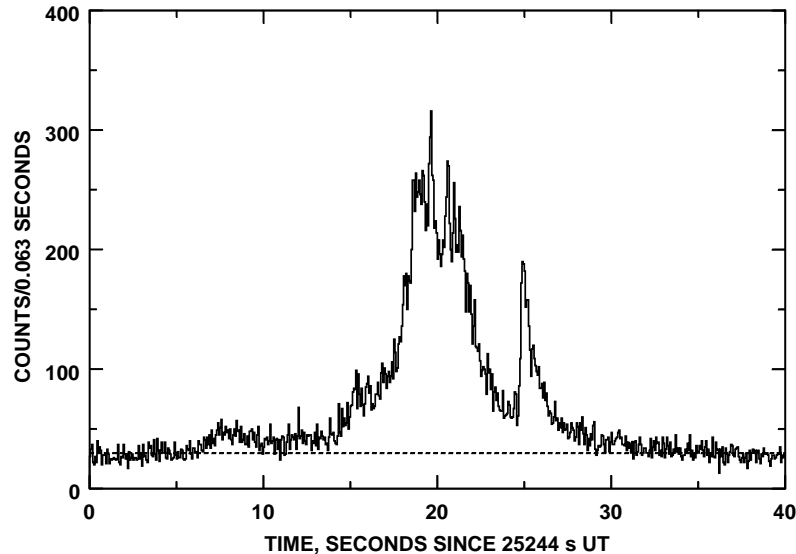


Fig. 15.1. A bright burst observed by the Ulysses GRB experiment on October 8 2002. The energy range is 25-150 keV. The dashed line indicates the background level. The 25-100 keV fluence of this event was $\approx 8 \times 10^{-5} \text{ erg/cm}^2$.

only the largest radio telescopes need apply: typical peak fluxes are at the milliJansky level.

Over the years, astronomers have become extremely adept at identifying GRB counterparts, to the point where redshifts have been measured in less than 8 hours from the time of the burst.

15.4 The bursting phase

15.4.1 *Gamma-ray burst lightcurves*

Gamma-ray bursts are, for a few seconds, the brightest objects in the gamma-ray sky. Figure 15.1 shows an example. Indeed, bursts are so bright that an uncollimated, unshielded detector with a surface area of only 20 cm^2 can detect a burst out to a redshift of $z=4.5$ (Andersen et al. 2000).

Burst durations span about 5 orders of magnitude, from 0.01 to 1000 s. The duration distribution displays a clear bimodality, with short bursts (durations ≈ 0.2 s) comprising around 25% of the total, and long bursts (durations ≈ 20 s) comprising the remainder (Mazets et al. 1981b; Dezalay et al. 1996; Norris et al. 1984; Hurley 1992; Kouveliotou et al. 1993). The distribution may be described by a lognormal function (McBreen et al. 1994). Apart from this, gamma-ray burst lightcurves are

generally very different from one burst to another, although certain morphological types have been noted. For example, about 7% of all bursts display a fast-rise, exponential decay morphology (Bhat et al. 1994). What determines the shape of the lightcurve in this and other morphologies is unknown.

In the lightcurves of very intense bursts, it is sometimes possible to detect a long, faint tail after the intense emission has ceased (Burenin et al. 1999). The count rate in the tail falls as a power law with time. This is a relatively short-lived (≈ 1000 s) gamma-ray afterglow. There is also evidence that the X-ray afterglow starts during the gamma-ray burst in many cases (Frontera et al. 2000).

15.4.2 *Energy spectra*

GRB energy spectra have been measured from ≈ 2 keV (Frontera et al. 2000) to 18 GeV (Hurley et al. 1994). Even at the highest energies accessible to spark chamber detectors, there is little or no evidence for spectral breaks. Indeed, there is even tantalizing evidence for TeV emission from one burst (Atkins et al. 2000). The spectra may be fit over a wide range with various models. One is the so-called “Band model” (Band et al. 1993) which has no particular physical derivation. Another is a synchrotron spectrum (Bromm & Schaefer 1999). An example of the latter is shown in figure 2. The spectrum in this figure is plotted in νF_ν units, which make it clear that the peak of the energy output during the burst, E_{peak} , is indeed at gamma-ray energies. The distribution of E_{peak} derived from BATSE data is quite narrow (Mallozzi et al. 1995), which is surprising considering the great diversity exhibited by most other GRB characteristics. The extent to which the E_{peak} distribution could be biased due to detector characteristics has been considered. There is presently no compelling evidence that a population of very high E_{peak} GRBs exists (Harris and Share 1998), although not all the phase space has been searched for such events. On the other hand, however, there *is* evidence for one or two classes of soft-spectrum bursts, called “x-ray rich GRBs” and “x-ray flashes” which appear to have all the characteristics of gamma-ray bursts, except for the gamma-rays above 20 keV or so (Heise et al. 2001). These may account for up to 30% of the total bursts. Some of these were in fact detected by BATSE (Kippen et al. 2001), but it seems plausible that many were not, leading to a possible bias against these events.

An interesting correlation exists between the time histories and the energy spectra of bursts: the short bursts have harder energy spectra than the long bursts (Dezalay et al. 1996; Kouveliotou et al. 1993). It is presently not understood why this is the case.

15.4.3 *GRB statistics*

It has been known for a long time that the spatial distribution of bursts is isotropic, to varying degrees of statistical uncertainty e.g. (Mazets et al. 1981a). It has similarly been known that the GRB number- intensity relation, or log N-log S curve, displayed a turnover at low intensities, that is, a paucity of weak events with respect to the $-3/2$ power law expected for a homogeneous distribution in Euclidean space (Mazets et al. 1981b). However, it was not until BATSE results became available that the situation was put into perspective and clarified (Pendleton et al. 1996; Paciesas et al. 1999). With unprecedented statistics and careful attention to

6 *Gamma-ray bursts*

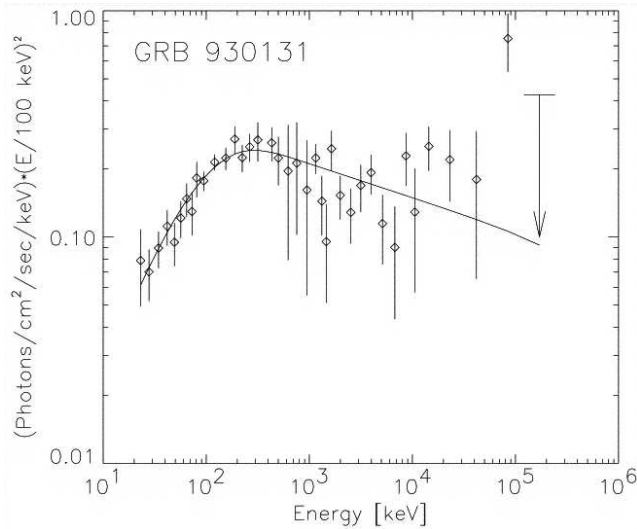


Fig. 15.2. The spectrum of GRB 930131 over four decades, and a synchrotron model fit (Bromm & Schaefer 1999). The spectrum is plotted in νF_ν units, which show the amount of energy per decade. The peak is at an energy $E_{\text{peak}} \approx 200\text{keV}$, and the energy output declines only slightly at higher energies.

instrumental details, the BATSE results confirmed the isotropy of bursts. They also confirmed the turnover in the log N-log S curve, albeit at much smaller intensities than before, indicating that the earlier turnover was due to instrumental effects (mainly the loss of sensitivity to weak events). The present results are consistent with a cosmological population of bursts (e.g. Stern, Atteia, & Hurley 2002). By some estimates, GRBs may occur out to redshifts of 10 or more, and current missions such as HETE are capable of detecting them to $z=8$ (Lamb and Reichart 2000).

It is obviously interesting to sample the GRB population below the BATSE trigger threshold. For example, if there were an epoch of early star formation in the Universe which gave rise to GRB-producing stellar deaths, this might be manifested by an increase in the log N-log S curve at low intensities. Two recent studies have succeeded in exploring the low intensity population (Kommers et al. 2000; Stern et al. 2001). By identifying bursts that were too weak to trigger the BATSE detector, they have effectively reduced the threshold by a factor of about 2. However, the conclusions of the studies differ; in one case, there appears to be evidence that the curve continues to rise at low intensities, suggesting that bursts continue to originate from earlier and earlier parts of the Universe, while in the other case, there is evidence for a flattening of the curve. It will require the next generation of GRB detectors to sort this out.

15.4.4 *Burst types and classes*

There are many *types* of gamma-ray bursts. They are often referred to as *classes*, but it is not known whether they actually originate from different kinds of explosions, or the explosions of different kinds of stars, as opposed to say, originating

from different viewing angles or other observing conditions. A brief, non-exhaustive summary of burst types follows.

- (a) Long and short bursts. The duration distribution is bimodal, and the energy spectra of the short bursts are harder than those of the long bursts. No radio, optical, or X-ray counterpart has been found for any short event (Hurley et al. 2002). It has been speculated that the short bursts might arise from neutron star- neutron star mergers (e.g. Macfadyen and Woosley 1999a), which could take place far from a host galaxy, and lack an ISM on which to produce a long-lived afterglow.
- (b) Dark bursts. While virtually all long bursts display X-ray afterglows, only about one-half of them have detectable radio or optical afterglows. There are various ways to hide intrinsically bright afterglows and make them undetectable, such as beaming them away from the observer, absorbing the light in the host galaxy, and placing the burst at high redshift. Yet another is to invoke a flat spectral shape (e.g. Hjorth et al. 2002). It is possible that more than one explanation is required.
- (c) Bursts possibly associated with supernovae. The first such event was GRB980425 (Galama et al. 1998c), a burst whose position and time of occurrence were both consistent with those of an optical supernova, 1998bw. In other cases, supernova-like bumps in the afterglow light curves have been identified and attributed to underlying supernovae (Bloom et al. 1999). In still other cases, there is no evidence for such components.
- (d) X-ray flashes (XRF's). These are bursts which resemble GRBs in almost every respect: durations, spatial distributions, etc. However, they display little or no emission above ≈ 25 keV (Heise et al. 2001). Possibly related to them are the X-ray rich GRBs, which display some gamma-ray emission (there is no widely accepted definition yet for just what ratio of X-ray flux to gamma-ray flux constitutes an XRF). One way to eliminate gamma- radiation is to redshift the burst. However, one X-ray rich GRB, 021004, has a redshift of only 1.6 (Fox et al. 2002), so this cannot be the only explanation.

15.5 GRB theory - the generic picture

The mechanism leading to the phenomenon of GRBs is yet a matter of debate. Nevertheless, some basic characteristics are well understood. Below, we show how the observed spectra, energies and timescales of GRBs have led to a generic model, the so-called fireball shock model that is almost independent of knowledge about the unknown 'inner engine'.

The extreme characteristics of GRBs, i.e. the observed large energies and short timescales, lead to a paradox, the 'compactness problem'. An energy of 10^{52} erg is released within a variability time $\delta T \sim 0.1$ s in the form of ≈ 1 MeV photons. This translates into a huge number of photons, $N = 10^{56}$. If we now assume that the energy is released in a small volume of linear dimension $R \leq c\delta T \sim 3 \times 10^9$ cm (which is naively required by the variability timescale), then the optical depth to pair creation would be the number of photons per unit area, multiplied by the Thomson

8 *Gamma-ray bursts*

cross section σ_T or

$$\tau \sim \sigma_T \frac{N}{4\pi R^2} \sim 3 \times 10^{11} \gg 1.$$

But, if that were true, it would imply that all the photons will have created pairs and thermalized. However, the observed spectrum of GRBs, as shown in the previous section is highly non-thermal!

The only known solution to the ‘compactness problem’ is relativistic motion (Paczynski 1986; Goodman, 1986). These effects have been considered in detail (Krolik & Pier 1991; Fenimore, Epstein, & Ho 1993; Baring & Harding 1997). A critical review of these as well as some new limits are given by Lithwick and Sari (2001). If the emission site is moving relativistically toward the observer with a Lorentz factor γ , then the optical depth is reduced compared to the stationary estimate, due to two effects. First, the size of the source can be larger by a factor of γ^2 . This will still produce variability over a short time scale given by $\delta T = R/\gamma^2 c$ since not all of the source is seen because the radiation for a relativistically moving object is beamed (see figure 15.3). Second, the photons in the local frame are softer by a factor of γ , and therefore only a small fraction of them, the ones at the high-energy tail of the GRB spectrum, have enough energy to create pairs. The combination of these two effects reduces the optical depth by a factor of $\sim \gamma^{6.5}$, where the exact power depends on the GRB spectrum (see Lithwick & Sari 2001). Therefore, the optical depth is reduced below unity, and the ‘compactness problem’ is solved, if the Lorentz factor is larger than about one hundred.

This solution to the compactness problem led to a three stage generic scenario for GRBs. First, a compact source releases about 10^{52} erg, in a small volume of space and on a short time scale. This large concentration of energy expands due to its own pressure (Mészáros & Rees 1993; Piran & Shemi 1993; Piran, Shemi, & Narayan 1993). If the rest mass that contaminates the site is not too large, $\leq 10^{-5} M_\odot$ (the requirement of a small baryonic load), this will result in relativistic expansion with $\gamma > 100$. Finally, at a large enough radius, the kinetic energy (bulk motion) of the expanding material is converted to internal energy and radiated, mainly in γ -rays. At this stage the system is optically thin and high energy photons can escape. We now discuss this third stage in some detail.

15.5.1 Internal vs. external shocks

Assume a flow carrying 10^{52} erg as kinetic energy. In order for this to produce photons, the kinetic energy must be converted back into internal energy and radiated away. The flow must therefore, at least partially, slow down. Two scenarios were proposed for this deceleration: external shocks (Mészáros & Rees 1993) and internal shocks (Narayan, Paczynski, & Piran 1992; Rees & Mészáros 1994). In the external shocks scenario, the relativistic material is running into some (external) ambient medium, possibly the interstellar medium (ISM) or a stellar wind that was emitted earlier by the progenitor. In the internal-shocks scenario the inner engine is assumed to emit an irregular flow consisting of many shells that travel with a variety of Lorentz factors and therefore collide with one another and thermalize part of their kinetic energy.

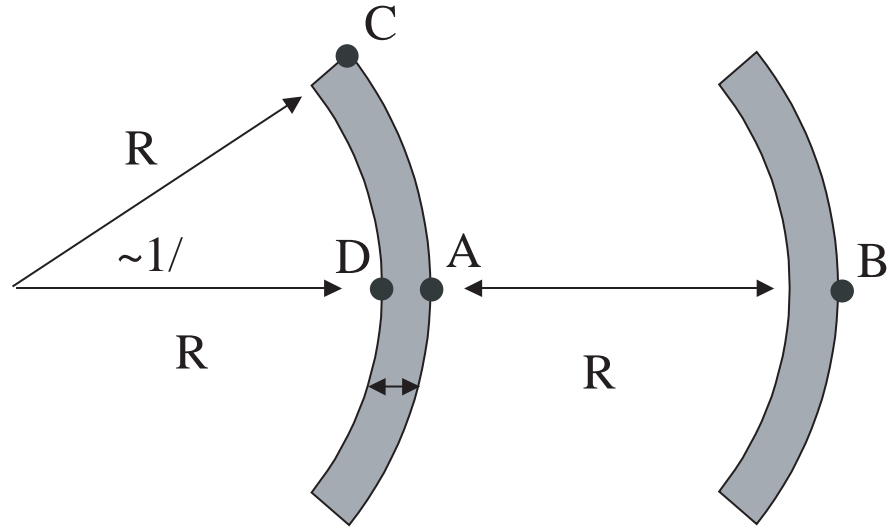


Fig. 15.3. Timescales from an expanding relativistic fireball. The gray area represents the observed section of the fireball that can be seen by an observer located far to the right. The angular opening of that section is $1/\gamma$ due to relativistic beaming. Consider the 4 photons emitted at points A, B, C, and D. Photons A, C and D were emitted simultaneously, but photon A will arrive at the observer first, since it is closer to the observer. The arrival-time delay of photons C and D with respect to photon A is simply given by the extra distance they have to travel. Therefore $\delta T_{C-A} = R(1 - \cos \theta)/c = R/2\gamma^2 c$, and $\delta T_{D-A} = \Delta/c \sim R/\gamma^2 c$, where we have used the fact that relativistic dynamics of fireballs imply $\Delta \sim R/\gamma^2$. Finally, photon B was emitted long after photon A (about a time R/c later than photon A); however, it is much closer to the observer, resulting in $\delta T_{B-A} = R/2\gamma^2 c$. All three timescales lead to the expression $R/\gamma^2 c$. A short observed variability time scale can therefore be obtained even for large radius, if the Lorentz factor is sufficiently high. The naive estimate of $R \leq c\delta T$ is, therefore, to be replaced by $R \leq \gamma^2 c\delta T$.

The property that proved to be very useful in constraining these two possibilities is the variability observed in many of the bursts. In the external shocks scenario, this variability is attributed to irregularities in the surrounding medium, e.g., clouds. Each time the ejecta run into a higher density environment, they produce a peak in the emission. In the internal shocks scenario, the source has to emit many shells, and when two of them collide a peak in the emission is produced. External shocks thus

require a complicated surrounding with a relatively simple source that explodes once, while internal shocks require a more complicated source that will explode many times to produce several shells. Due to these very different requirements on the source, the question of internal or external shocks is of fundamental importance in understanding the nature of the phenomenon.

The size of the clouds that the ejecta run into, in the external-shocks scenario, has to be very small in order to produce peaks that are narrower than the duration of the burst (Fenimore, Madras, & Nayakchin 1996). Sari & Piran (1997a) gave the following argument. The size of the clouds has to be smaller than $R/N\gamma$ to produce peaks that are narrower by a factor of N than the duration of the burst. The number of clouds should be smaller than N otherwise pulses arriving from different clouds will overlap and the amplitude of the variability will be reduced. Finally, due to relativistic beaming, the observable area of the ejecta is $(R/\gamma)^2$. The maximal efficiency of the external shocks scenario is therefore given by

$$\frac{\text{cloud area} \times \text{number of clouds}}{\text{observed shell area}} \leq \frac{1}{N} \sim 1\%. \quad (15.1)$$

Since in many bursts $N > 100$, external shocks have a severe efficiency problem in producing highly variable bursts. The problem is even more dramatic if long quiescent periods, which are observed in many bursts (Nakar & Piran 2002), are taken into account. Also, other predictions of external shocks are inconsistent with the observed temporal profile (Ramirez-Ruiz & Fenimore 1999). Moreover, the density ratio between the clouds and their surroundings has to be huge, of the order of $\gamma N^2 \sim 10^6$, in order for the ejecta to be slowed down mainly by the dense clouds rather than by the low density medium that they are embedded in. Finally, we mention that despite the above arguments, some still favor other scenarios (Dermer & Mitman 1999; Dar & DeRujula 2000).

Internal shocks do not suffer from these problems. Detailed calculations show that the observed temporal structure from internal shocks closely follows the operation of the inner engine that generated the shells (Kobayashi, Piran, & Sari 1997). In this scenario, the source must be variable on time scales shorter than a second and last for as long as 100 seconds, just as the bursts themselves.

The efficiency of internal shocks is largely determined by the ratio of Lorentz factors between different shells which are colliding with each other. The larger the ratio, the larger the efficiency. A simple scenario that demonstrates this is the case of two equal mass shells with Lorentz factors $\gamma_1 \gg \gamma_2 \gg 1$. Conservation of energy and momentum in a collision between the shells leads to a Lorentz factor which is the geometric mean of the initial ones $\sqrt{\gamma_1\gamma_2}$. Therefore, the energy left in the system as non-thermal is a small fraction $\sqrt{\gamma_2/\gamma_1}$ of the initial energy. Beloboradov (2000) has argued that if large Lorentz factor ratios are allowed, the internal shock efficiency is only limited by the fraction of energy in the shock given to the radiating electrons. Kobayashi and Sari (2001) have then shown that multiple collisions between shocks may result in ‘ultra efficient’ internal shocks, in the sense that even more than the fraction of energy given to electrons can be radiated away.

The mechanism by which the thermal energy produced by internal shocks is converted to radiation is almost certainly synchrotron and inverse Compton, since these

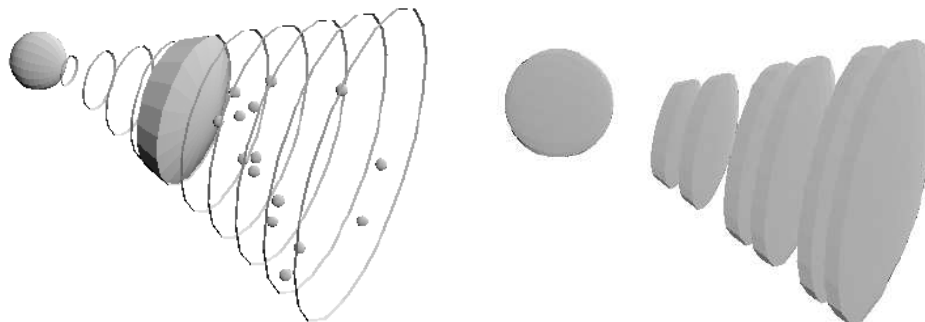


Fig. 15.4. Producing variability by external shocks (left) or internal shocks (right). In the external shocks scenario, the variability is produced by irregularities in the surrounding. If the surrounding consists of a low density medium that contains high density clouds, then whenever the shell hits one of the clouds a peak in the emission is produced. The number of clouds within the observable cone (of angular size $1/\gamma$ due to relativistic beaming) should therefore roughly be the number of observed peaks. The source itself, in this model, needs to produce only a single shell in a single (simple) explosion. However, the external shocks scenario has low efficiency, due to the small total surface area of the clouds when compared to the area of the shell. In the internal-shocks case, the temporal structure arises from the source, i.e. the source produces a more complex explosion. There is no efficiency problem, provided that the relative Lorentz factor between shells is large.

are the dominant radiation mechanisms at the low densities involved. While both mechanisms probably take place, it is actually not very clear which of the two produces the observed radiation. Synchrotron emission is for several reasons preferred (Sari, Narayan & Piran 1996; Sari & Piran 1997b) and inverse Compton probably produces a higher energy component.

15.6 The afterglow: theory

After the internal shocks produce the GRB, the shell interacts with the surrounding medium and decelerates. Again it emits radiation by synchrotron and inverse Compton. As the flow decelerates, the emission shifts to lower and lower frequencies. This emission, the afterglow, may last on detectable levels for years after the GRB itself!

Afterglow was predicted well before it was observed (Paczýński & Rhoads 1993; Katz, 1994; Vietri, 1997; Mészáros & Rees 1997). The afterglow theory is relatively simple. It deals with the emission on timescales much longer than that of the GRB. The details of the complex initial conditions are therefore forgotten and the condition of the GRB remnant can be described by a self-similar solution with a small number of parameters, such as the total energy and the external density. It is assumed that the electrons are accelerated by the shock into a power-law distribution of electron Lorentz factors $N(\gamma_e) \propto \gamma_e^{-p}$ for $\gamma_e > \gamma_m$. The lower cutoff γ_m of this distribution is set by the assumption that the electrons acquire a fixed fraction, ϵ_e , of the thermal energy. It is also assumed that a considerable magnetic field is built behind the

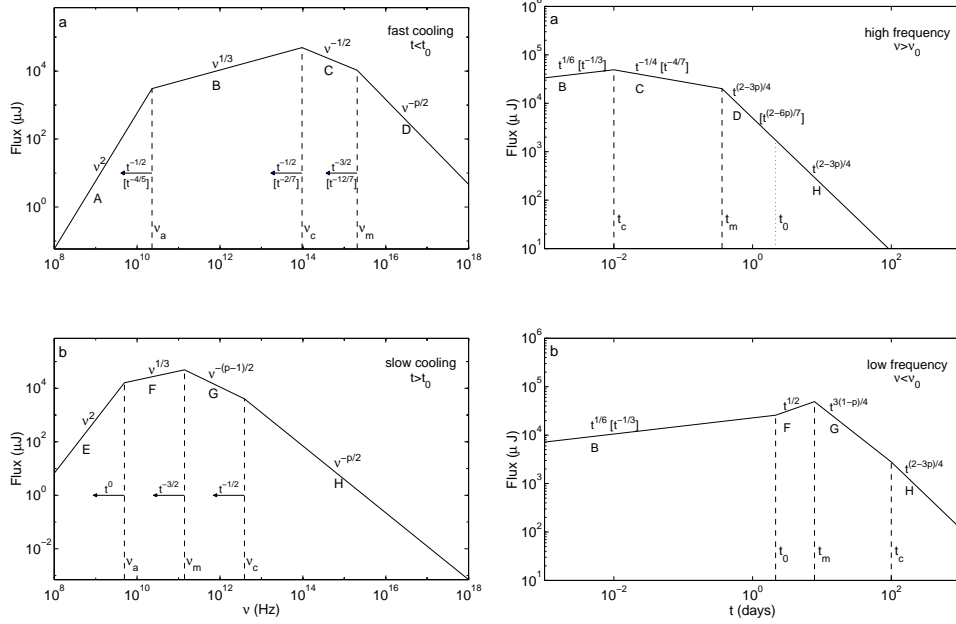


Fig. 15.5. Theoretical spectra (left) and light curves (right) of synchrotron emission from a powerlaw distribution of electrons for the case of a constant density ambient medium and a spherical explosion. For most cases $p = 2.2 - 2.5$ fits the observed spectra and lightcurves well .

shock, which is again characterized by a certain fraction ϵ_B of equipartition. The energy density behind a relativistic shock is given by $4\gamma^2 n m_p c^2$, where $n = n_1 \text{ cm}^{-3}$ is the proton number density behind the shock, γ is the Lorentz factor of the fluid behind the shock, and m_p is the proton mass. These equipartition assumptions then result in

$$\gamma_m = \frac{p-2}{p-1} \frac{m_p}{m_e} \epsilon_e \gamma \cong 630 \epsilon_e \gamma \quad (15.2)$$

$$B = 0.4 \sqrt{\epsilon_B n_1} \gamma \text{ Gauss,} \quad (15.3)$$

where B is the magnetic field, and m_e is the electron mass. The relativistic electrons then emit synchrotron radiation which produces the observed afterglow. The broadband spectrum of such afterglow emission was given by Sari, Piran & Narayan (1998).

The afterglow synchrotron spectrum can be fully described by the electron energy index p , the peak flux F_m and three characteristic frequencies (ν_m, ν_c, ν_a):

(I) ν_m is the synchrotron frequency of the minimum energy electron, with Lorentz factor γ_m . From synchrotron theory $\nu_m \cong (eB/2\pi m_e c) \gamma_m^2$ in the local frame of the fluid; here e is the electron charge. Transforming this to the observer frame (blue

shifted by the Lorentz factor and redshifted by a factor of $[1+z]$ and using equations 15.2 and 15.3 we obtain

$$\nu_m = 1.4 \times 10^{13} \text{Hz} (1+z)^{-1} \left(\frac{\epsilon_e}{0.1}\right)^2 \left(\frac{\epsilon_B}{0.1}\right)^{1/2} \left(\frac{\gamma}{10}\right)^4 n_1^{1/2}. \quad (15.4)$$

(II) The cooling time of an electron is inversely proportional to its Lorentz factor γ_e . Therefore, electrons with a Lorentz factor higher than a critical Lorentz factor $\gamma_e > \gamma_c$ cool on the dynamical timescale of the system. This characteristic Lorentz factor is given by the condition $\sigma_T c \gamma^2 \gamma_c^2 B^2 t \gamma / 6\pi(1+z) = \gamma_c m_e c^2$, and corresponds to the ‘cooling frequency’

$$\nu_c = 1.2 \times 10^{13} \text{Hz} (1+z) \left(\frac{\epsilon_B}{0.1}\right)^{-3/2} \left(\frac{\gamma}{10}\right)^{-4} n_1^{-3/2} t_{days}^{-2}, \quad (15.5)$$

where t_{days} is the observer time in days. Here we have also taken into account that time is redshifted.

(III) Below some critical frequency ν_a the flux is self-absorbed and is given by the Rayleigh-Jeans portion of a blackbody spectrum*. The self-absorption frequency is given by

$$\nu_{sa} = 93 \text{GHz} (1+z)^{-13/5} \left(\frac{\epsilon_B}{0.1}\right)^{6/5} \left(\frac{\gamma}{10}\right)^{28/5} n_1^{9/5} t_{days}^{8/5}, \quad (15.6)$$

if $\nu_c < \nu_m$, and by

$$\nu_{sa} = 87 \text{GHz} (1+z)^{-8/5} \left(\frac{\epsilon_e}{0.1}\right)^{-1} \left(\frac{\epsilon_B}{0.1}\right)^{1/5} \left(\frac{\gamma}{10}\right)^{8/5} n_1^{4/5} t_{days}^{3/5}, \quad (15.7)$$

if $\nu_c > \nu_m$.

(IV) The normalization of the spectrum is given by the total number of radiating electrons $4\pi R^3 n_1 / 3$ times the peak flux from a single electron, resulting in

$$F_m = 220 \text{mJy} (1+z)^{-2} d_{L,28}^{-2} \left(\frac{\epsilon_B}{0.1}\right)^{1/2} \left(\frac{\gamma}{10}\right)^8 n_1^{3/2} t_{days}^3, \quad (15.8)$$

where $d_{L,28}$ is the luminosity distance in units of 10^{28}cm .

The broadband spectrum of the well studied GRB 970508 (Galama et al. 1998b) is in very good agreement with the theoretical picture. Note that the derivation above is quite general. It does not depend either on the surrounding density profile or on the geometry of the event. Both these effects are hidden in the evolution of the fluid Lorentz factor γ , and the particle density n_1 as a function of time.

The evolution of this spectrum as a function of time depends on the hydrodynamics. The simplest, which describes the observations in some cases quite well, is the adiabatic model with a constant density surrounding medium. The rest mass collected by the shock at radius R is about $R^3 \rho$, where ρ is the mass density. On average, the particles move with a Lorentz factor of γ^2 in the observer frame (one

* Granot, Piran & Sari (2000b) have found that if $\nu_c < \nu_m$, then the self-absorption frequency actually splits into two: ν_{ac} and ν_{sa} , where an optical depth of unity is produced by non-cooled electrons and all electrons, respectively. In between these two frequencies the spectral slope is $\nu^{11/8}$.

14 *Gamma-ray bursts*

factor of γ is the bulk motion and the other is the random thermal motion). Therefore, the total energy is given by $E \propto \gamma^2 R^3 \rho c^2$. Assuming that the radiated energy is negligible compared to the energy of the flow, we obtain that $\gamma \propto R^{-3/2}$ or in terms of the observer time, $t = R/\gamma^2 c$, we get $\gamma \propto t^{-3/8}$.

$$\nu_m = 6 \times 10^{15} \text{ Hz } (1+z)^{1/2} E_{52}^{1/2} \epsilon_e^2 \epsilon_B^{1/2} t_{\text{days}}^{-3/2}$$

$$\nu_c = 9 \times 10^{12} \text{ Hz } (1+z)^{-1/2} \epsilon_B^{-3/2} n_1^{-1} E_{52}^{-1/2} t_{\text{days}}^{-1/2}$$

$$\nu_{sa} = 2 \times 10^9 \text{ Hz } (1+z)^{-1} \epsilon_e^{-1} \epsilon_B^{1/5} n_1^{3/5} E_{52}^{1/5}$$

$$F_m = 20 \text{ mJy } (1+z) \epsilon_B^{1/2} n_1^{1/2} E_{52}^{-2} d_{L28}^{-2}$$

If, on the other hand (Chevalier & Li 1999), the density drops as R^{-2} (as is expected if the surrounding is a wind produced earlier by the progenitor of the burst) we get $\gamma \sim t^{-1/4}$. Choosing the parameter A_* to define the normalization of the density as $\rho R^2 = A_* 5 \times 10^{11} A_* \text{ gr/cm}$ results in

$$\nu_m = 1.7 \times 10^{14} \text{ Hz } (1+z)^{1/2} E_{52}^{1/2} \epsilon_e^2 \epsilon_B^{1/2} t_{\text{days}}^{-3/2}$$

$$\nu_c = 7 \times 10^{11} \text{ Hz } (1+z)^{-3/2} \epsilon_B^{-3/2} A_*^{-2} E_{52}^{1/2} t_{\text{days}}^{1/2}$$

$$\nu_{sa} = 1.5 \times 10^{10} \text{ Hz } (1+z)^{-2/5} \epsilon_e^{-1} \epsilon_B^{1/5} A_*^{6/5} E_{52}^{-2/5} t_{\text{days}}^{-3/5}$$

$$F_m = 180 \text{ mJy } (1+z)^{3/2} \epsilon_B^{1/2} A_* E_{52}^{1/2} t_{\text{days}}^{-1/2} d_{L28}^{-2}$$

These simple scalings, for the case of a constant density ambient medium, lead to the spectral evolution given in Figure 15.5. The derivations above use a very simple description of the flow. It represents the fluid as if it had a single magnetic field strength and a single Lorentz factor γ and all of the material is moving directly towards the observer. Also, a very approximate description of the synchrotron emission was used. In reality, of course, the situation is more complicated. There are two effects that must be taken into account. The most dramatic one is the fact that matter slightly off the line of sight does not move directly towards the observer (Waxman 1997b; Panaitescu & Mészáros 1998; Sari 1998). The amount of Lorentz boost from that matter is reduced. Secondly, fluid elements at different distances from the shock have somewhat different Lorentz factors, magnetic fields and electron energies. These variations can be estimated using the self-similar solution of Blandford and McKee (1976). The outcome of these more detailed calculations are the same scaling laws, but with a more accurate coefficient for the break frequencies as well as an estimate of the shape of the spectrum around each break frequency (Granot, Piran & Sari 2000; Gruzinov & Waxman 1999; Granot, Piran & Sari 1999). The equations

given above already take these effects into account, and the coefficients given are accurate for $p = 2.2$.

The above scalings assumed adiabatic evolution. At first sight one might think that if the fraction of energy given to the electrons, ϵ_e , is less than unity, then perhaps only a small fraction of the energy can be radiated away. However, the same fireball energy is given again and again to newly shocked electrons. Each time, a fraction ϵ_e can be radiated away, and the overall effect can be large, much above the fraction ϵ_e . Energy losses during the cooling phase can be taken into account (Sari 1998; Cohen, Piran & Sari 1998) using $dE/dR = -(16\pi/3)R^2\epsilon_e\gamma^2m_p c^2n$. This results in $E = E_0 \times (t/t_0)^{-17\epsilon_e/12}$ for a constant density environment and $E = E_0 \times (t/t_0)^{-3\epsilon_e/2}$ for a wind environment. These effects are not taken into account in many models but may actually have a significant impact if ϵ_e is not too far below unity. In the case of GRB 000926, energy losses appear to have reduced the energy of the system by a factor of 5 (Harrison et al. 2001).

Given the above hydrodynamic evolution, one can construct light curves at any given frequency. These will also consist of power laws, changing from one power law to another once the break frequencies pass through the observed band. These predicted power law lightcurves and spectra are in fair agreement with afterglow observations (see Section 15.7).

We have so far considered synchrotron radiation only. Since the optical depth of the system is small, most of the synchrotron photons emitted can be observed. Still, inverse Compton can affect the system in two ways. First, it may add an observable high-energy component. This requires a moderately high density. Second, it may provide an important cooling mechanism, and alter the synchrotron spectrum by its effect on ν_e . The ratio of the inverse Compton (IC) to synchrotron luminosity (a measure of their relative importance for cooling) can be computed very generally (Sari, Narayan, & Piran 1996), in a way that does not deal with the details of the spectrum, but depends only on the underlying physical properties of the expanding shock wave. We generalize the derivation given by Sari, Narayan, & Piran (1996) to describe both fast and slow cooling regimes by introducing a parameter η , equal to the fraction of the electron energy that was radiated away (via both synchrotron and IC emission) (Sari & Esin 2001). Then the ratio of luminosities, in the limit of single scattering, is given by

$$x \equiv \frac{L_{IC}}{L_{syn}} = \frac{U_{rad}}{U_B} = \frac{U_{syn}}{U_B} = \frac{\eta U_e / (1+x)}{U_B} = \frac{\eta \epsilon_e}{\epsilon_B (1+x)}, \quad (15.9)$$

where U_{syn} , U_B and U_e are the energy density of synchrotron radiation, magnetic field and relativistic electrons, respectively. Note that in general $U_{syn} = \eta\beta U_e / (1+x)$, where β is the velocity of material behind the shock front (in the frame of the shock); however, for a relativistic shock $\beta \cong 1$. The importance of inverse Compton therefore diminishes quickly when the fireball becomes non-relativistic.

Solving Eq. (15.9) for x we obtain

$$x = \frac{-1 + \sqrt{1 + 4\frac{\eta\epsilon_e}{\epsilon_B}}}{2} \cong \begin{cases} \frac{\eta\epsilon_e}{\epsilon_B}, & \text{if } \frac{\eta\epsilon_e}{\epsilon_B} \ll 1, \\ \left(\frac{\eta\epsilon_e}{\epsilon_B}\right)^{1/2}, & \text{if } \frac{\eta\epsilon_e}{\epsilon_B} \gg 1. \end{cases} \quad (15.10)$$

Modeling afterglow data often suggests that $\epsilon_e \gg \epsilon_B$ and therefore inverse Compton may be of importance.

15.7 The afterglow revolution

Motivated by the prediction of a late-time softer radiation (the afterglow), several groups executed rapid radio follow-up observations of GRB error boxes. Detection of a radio afterglow seemed most promising. Not only does the large field of view match well with the large error boxes (several degrees) that were then available on short time scales (within a day), but maximum light was also expected to occur later at longer wavelengths. The best (pre-BeppoSAX era) limits on such afterglow radio emission were obtained for GRB 940301. This GRB triggered an extensive multi-wavelength campaign with ground based optical and radio observatories from the BATSE / COMPTEL / NMSU Rapid Response Network (McNamara et al. 1995). No obvious candidate radio counterparts were found (Frail et al. 1994; Koranyi et al. 1995; Galama et al. 1997a).

15.7.1 *The first identifications*

The breakthrough came in early 1997, when the Wide-Field Cameras (WFCs; Jager et al. 1993) onboard the Italian-Dutch satellite BeppoSAX (Piro, Scarsi & Butler 1995) obtained their first quickly available (within hours) accurate positions of GRBs (several arcminutes). This allowed rapid follow-up observations which led to the discoveries of X-ray (Costa et al. 1997), optical (van Paradijs et al. 1997), millimeter (Bremer et al. 1998) and radio (Frail et al. 1997) counterparts of GRBs. These observations quickly settled the distance controversy. The first transient optical counterpart, of GRB 970228, is in a faint galaxy with $\sim 0.8''$ diameter (Sahu et al. 1997). And, detection of absorption features in the OT's spectrum of GRB 970508 (Metzger et al. 1997) established that this event was at a redshift greater than $z = 0.835$. GRBs come from 'cosmological' distances and are thus extremely powerful events. They are by far the most luminous photon sources in the Universe, with (isotropic equivalent) peak luminosities in γ rays up to 10^{52} erg/s, and total energy budgets up to several 10^{53-54} erg (Kulkarni et al. 1998; Kulkarni et al. 1999a) (but see Section 15.8 and 15.9 for a discussion of collimated outflow, which reduces the inferred total energy). Within the first day, the optical emission is usually brighter than 20th magnitude (some 10 mag brighter [absolute] than the brightest supernovae) and therefore small telescopes can play an important role in measuring the lightcurve. Today, a large worldwide collaboration is observing these events and the data are submitted to the Gamma-Ray Burst Coordinates Network in near-real time, allowing other observatories to react rapidly.

15.7.2 *Confirmation of the relativistic blast-wave model*

A stringent test of the relativistic blast wave model came with the discovery of X-ray (Costa et al. 1997) and optical afterglow following GRB 970228 (van Paradijs et al. 1997; Galama et al. 1997b). The X-ray and optical afterglows of GRB 970228 show a power-law temporal decay; this is a trend observed in all subsequent X-ray and optical afterglows, with power-law exponents in the range 1 to 2.

Let us first concentrate on the forward shock and assume slow cooling (the bulk of the electrons do not radiate a significant fraction of their own energy and the evolution is adiabatic); this appears applicable to some observed GRB afterglows at late times ($t > 1$ hr). The simplest assumption is that of spherical symmetry and a constant ambient density. As both the afterglow's spectrum and the temporal evolution of the break frequencies ν_a, ν_m, ν_c are, in the relativistic blast wave model, power laws (see Section 15.6), the evolution of the flux is also a power law in time. For example, for $\nu_m \leq \nu \leq \nu_c$, the decay of the flux is $F_\nu \propto t_{\text{obs}}^{-3(p-1)/4}$, and the power law spectral slope α relates to the spectral slope β as $\alpha = -3/2\beta$. Several authors (Wijers, Rees, & Mészáros, 1997; Reichart 1997; Waxman 1997a) showed that to first order this model describes the X-ray and optical afterglow of GRB 970228 very well.

GRB 970508 was the first GRB with a radio counterpart (Frail et al. 1997). The radio light curves (8.5 and 4.9 GHz) show large variations on time scales of less than a day, but these damp out after one month. This finds a viable explanation in interstellar scintillation (stochastic refraction and diffraction by the fluctuations in the interstellar medium electron density between the source and the observer). The damping of the fluctuations can then be understood as the effect of source expansion on the diffractive interstellar scintillation. Thus a source size of roughly 10^{17} cm was derived (at 3 weeks), corresponding to a mildly relativistic expansion of the shell (Frail et al. 1997).

GRB 970508 remains one of the best observed afterglows: the radio afterglow was visible at least 368 days (and with 2.5σ significance on day 408.6 (Frail, Waxman & Kulkarni 2000)), and the optical afterglow up to ~ 450 days (e.g. Fruchter et al. 2000; Galama et al. 1998a; Castro-Tirado et al. 1998). In addition millimeter (Bremer et al. 1998), infrared and X-ray (Piro et al. 1998) counterparts were detected. These multiwavelength observations allowed the reconstruction of the broad radio to X-ray spectrum for this GRB (Galama et al. 1998b) Galama et. al. (1998b) found that the 'standard' model provides a successful and consistent description of the afterglow observations over nine decades in frequency, ranging in time from the event until several months later. The synchrotron afterglow spectrum of this GRB allows measurement of the electron energy spectrum p , the three break frequencies (ν_a, ν_m and ν_c), and the flux at the peak, F_m . For GRB 970508 the redshift z is also known, and all blast wave parameters could be deduced: the total energy (per unit solid angle) $E = 3.5 \times 10^{52}$ erg, the ambient (nucleon) density $n_1 \approx 5$, the fraction of the energy in electrons $\epsilon_e \approx 0.5$ and that of the magnetic field $\epsilon_B = 0.01$ (Wijers & Galama 1999; Granot, Piran, & Sari 1999). The numbers themselves are uncertain by an order of magnitude, but the result shows that the 'standard' model fits the expectations very well.

Following these first attempts at modeling the broad-band afterglow more detailed modeling efforts have been made. For example, Panaitescu and Kumar (2001a) have modeled a sample of GRBs with relativistic jets (see Section 15.8 and 15.9 for a detailed discussion on jets) and find: typical energies of $10^{50} - 10^{51}$ erg, ambient densities ranging from $10^{-3} - 10$ cm $^{-3}$, beaming angles ranging between $1^\circ - 4^\circ$, and that a wind-like ambient medium can in some cases be ruled out GRB 000301C was modeled with a hard electron-energy distribution (Panaitescu 2001); $p = 1.5$) (but see

Berger et al. 2000) and GRB 010222 also requires a hard electron energy distribution (Galama et al. 2001). Evidence has been presented for an inverse Compton emission component in the afterglow of GRB 000926 (Harrison et al. 2001).

The highly relativistic nature of the GRB source (Galama et al. 1999) can once more be seen in the extreme brightness temperature of the GRB 990123 optical flash (Akerlof et al. 1999) $T_b \geq 10^{17}$ K; see Sect 15.11) which by far exceeds the Compton limit of 10^{12} K. In this case the optical signal from GRB 990123 was some 18 mag brighter (absolute) than the brightest supernovae. The extreme brightness can be explained by emission from the reverse shock (see Section 15.11).

15.8 Collimated outflow (jets): theory

The hydrodynamic evolution described in Section 15.6, assumed spherical symmetry. However, many astrophysical phenomena, especially those involving extreme energetics, are not spherical but in the form of jets. As we will see, this is most probably the case also for GRBs.

Jets have been discussed extensively in the context of GRBs. First, the similarity between some of the observed features of blazars and AGNs led to the speculation that jets also appear in GRBs (Paczynski 1993). Second, the regions emitting the GRBs as well as the afterglow must be moving relativistically. The emitted radiation is strongly beamed, and we can observe only a region with an opening angle $1/\gamma$ off the line of sight. Emission outside of this very narrow cone is not observed. These considerations have led to numerous speculations on the existence of jets and to attempts to search for the observational signature of jets both during the GRB phase (Mao & Yi 1994) and in the context of the afterglow (Rhoads 1997; Rhoads 1999; Mészáros, Rees & Wijers 1998).

We begin by clarifying some of the confusing terminology. There are two distinct but related effects. The first, ‘*jets*’, describes scenarios in which the relativistic flow emitted from the source is not isotropic but collimated into a finite solid angle. The term jet refers to the geometrical shape of the relativistic flow emitted from the inner engine. The second effect is that of ‘*relativistic beaming*’. The radiation from any object that is radiating isotropically in its own rest frame, but moving with a large Lorentz factor γ in the observer frame, is beamed into a small angle $1/\gamma$ around its direction of motion. This is an effect of special relativity. It has nothing to do with the ejecta’s geometry (spherical or jet) but only with the fact that the ejecta is moving relativistically. The effect of relativistic beaming allows an observer to see only a small angular extent, of size $1/\gamma$ centered around the line of sight. Since we know the flow is ultra-relativistic (initially $\gamma > 100$), there is no question that the relativistic beaming effect is always relevant for GRBs. The question we are interested in is that of the existence of ‘jets’.

The idealized description of a jet is a flow that occupies only a conical volume with half opening angle θ_0 . In fact, the relativistic dynamics is such that the width of the material in the direction of its propagation is much smaller than its distance from the source by a factor of $1/\gamma^2$. The flow, therefore, does not fill the whole cone. Instead it occupies only a thin disk at its base, looking more like a flying pancake (Piran 1999) (see Figure 15.4). If the ‘inner engine’ emits two such jets in opposite directions then the total solid angle towards which the flow is emitted is $\Omega = 2\pi\theta_0^2$.

Whether the relativistic flow is in the form of a jet or a sphere has three important implications.

The Total Emitted Energy. Optical observations of afterglows enabled redshift determinations, and therefore reasonably accurate estimates of the distance, D , to these events (the uncertainty is now in the cosmological parameters of the Universe). The so called ‘isotropic energy’ can then be inferred from the fluence F (the total observed energy per unit area at earth) as $E_{iso} = 4\pi D^2 F$ (taking cosmological corrections into account, $D = d_L/\sqrt{1+z}$ where d_L is the luminosity distance and z is the redshift). The numbers obtained in this way range from 10^{51} erg to 10^{54} erg with the record of 3×10^{54} erg held by the famous GRB 990123. These huge numbers approach the equivalent energy of a solar mass, all emitted in a few tens of seconds!

These calculations assumed that the source emitted the same amount of energy in all directions. If instead the emission is confined to some solid angle Ω then the true energy is $E = \Omega D^2 F$. As we show later Ω is very weakly constrained by the GRB itself and can be as low as 10^{-6} . If so the true energy in each burst $E \ll E_{iso}$. We will show later that interpretation of the multi-wavelength afterglow lightcurves indeed indicates that some bursts are jets with solid angles considerably less than 4π . The isotropic energy estimates may be fooling us by a few orders of magnitudes! Clearly this is of fundamental importance when considering models for the sources of GRBs.

The Event Rate. In its glory days, BATSE detected about one burst per day. With the help of several redshift measurements, or alternatively, with the use of the cumulative brightness distribution (the Log N-Log S curve), this translates to about 10^{-7} bursts per year per galaxy or 0.5 bursts/Gpc $^{-3}$ /year (Schmidt 1999; Schmidt 2001). However, if the emission is collimated to $\Omega \ll 4\pi$ then we do not see most of the events. The true event rate is then larger than that measured by BATSE by a factor of $4\pi/\Omega$. Again this is of fundamental importance. Clearly, the corrected GRB event rate must not exceed that of compact binary mergers or the birth rate of massive stars if these are to produce the majority of the observed GRBs

The Physical Ejection Mechanism. Different physical models are needed to explain collimated and isotropic emission. For example, in the collapsar model (e.g. MacFadyen & Woosley 1999b), relativistic ejecta that are believed to create the GRB are produced only around the rotation axis of the collapsing star with a half opening angle of about $\theta_0 \cong 0.1$. Such models would have difficulties explaining isotropic bursts as well as very narrow jets.

15.8.1 The jet-break

As the afterglow evolves, γ decreases and it will eventually fall below the initial inverse opening angle of the jet. The observer will notice that some of the sphere is missing from the fact that less radiation is observed. This effect alone will produce a significant break, steepening the lightcurve decay by a factor of $\gamma^2 \propto t^{-3/4}$ even if the dynamics of each fluid element has not changed. The transition should occur at the time t_{jet} when $1/\gamma \cong \theta_0$. Observing this time can therefore provide an estimate of the jet’s opening angle according to

20 *Gamma-ray bursts*

$$t_{\text{jet}} \approx 6.2\text{hr}(1+z)(E_{52}/n_1)^{1/3}(\theta_0/0.1)^{8/3}. \quad (15.11)$$

Additionally, Rhoads (1999) has shown that at about the same time (see however Panaitescu & Mészáros 1999; Mészáros & Rees 1999; Moderski, Sikora & Bulik 2000), the jet will begin to spread laterally so that its opening angle $\theta(t) \sim 1/\gamma$. The ejecta now encounter more surrounding matter and decelerate faster than in the spherical case. The Lorentz factor then decays exponentially with the radius and as $\gamma \propto t^{-1/2}$ with observed time. Taking this into account, the observed break is even more significant. The slow cooling spectrum given in Figure 15.5 evolves with decreasing peak flux $F_m \propto t^{-1}$ and the break frequencies evolve as $\nu_m \propto t^{-2}$, $\nu_c \propto t^0$ and $\nu_a \propto t^{-1/5}$. This translates to a temporal decay at a given frequency given in Table 15.1.

	spectral index $\beta, F_\nu \propto \nu^{-\beta}$	light curve index $\alpha, F_\nu \propto t^{-\alpha}$	
		sphere	jet
$\nu < \nu_a$	$\beta = -2$	$\alpha = -1/2$	$\alpha = 0$
$\nu_a < \nu < \nu_m$	$\beta = -1/3$	$\alpha = -1/2$	$\alpha = 1/3$
$\nu_m < \nu < \nu_c$	$(p-1)/2 \cong 0.7$	$\alpha = 3(p-1)/4 \cong 1.05$ $\alpha = 3\beta/2$	$\alpha = p \cong 2.4$ $\alpha = 2\beta + 1$
$\nu > \nu_c$	$p/2 \cong 1.2$	$\alpha = (3p-2)/4 \cong 1.3$ $\alpha = 3\beta/2 - 1/2$	$\alpha = p \cong 2.4$ $\alpha = 2\beta$

Table 15.1. *The spectral index β and the temporal index α as functions of p for a spherical and a jet-like evolution. Typical values are quoted using $p = 2.4$. The parameter-free relation between α and β is given for each case (eliminating p). The difference in α between a jet and a sphere is always substantial at all frequencies.*

The jet break is a hydrodynamic one. It should therefore appear at the same time at all frequencies - an achromatic break*. Though an achromatic break is considered to be a strong signature of a jet, one should keep in mind that any other hydrodynamic transition will also produce an achromatic break. To name a few: the transition from relativistic to non-relativistic dynamics, a jump in the ambient density or the supply of new energy from slower shells that catch up with the decelerated flow. However, the breaks produced by the transition from a spherical-like evolution (when $1/\gamma < \theta_0$) to a spreading jet have a well defined prediction for the change in the temporal decay indices. The amount of break depends on the spectral regime that is observed. It can be seen from Table 15.1 that the break is substantial ($\Delta\alpha > 0.5$ in all regimes) and should be easily identified.

* Sari 1997 (Sari 1997), argued that there may be about a factor of two difference in the effective transition time between the four different spectral regimes (e.g. below or above ν_m) due to the fact that the emission in these different regimes weighs contributions from various emission radii differently

15.9 Observational evidence for collimated outflow (jets)

The theory of jet evolution and of the resulting light curves was worked out before evidence for jets was obtained. In fact, Rhoads (1999), has used this theory to constrain the amount of collimation in GRB 970508, which did not show any significant steepening of the afterglow lightcurve. He concluded that the opening angle of a jet, if it exists, must be more than 30 degrees. We note that if the jet's opening angle is of order unity, the total energy may still be about an order of magnitude lower than the isotropic estimate. However, in this case the break will be 'hidden' as it will overlap the transition to non-relativistic dynamics. Based on late time radio data, it was suggested that this is the case for GRB 970508 (Frail, Waxman & Kulkarni 2000).

The first claim for narrow jets in GRBs came from Sari, Piran and Halpern (1999). They noted that the observed decays in GRB afterglows that do not show a break either have a shallow slope $F_\nu \propto t^{-1.2}$ or a very steep slope $F_\nu \propto t^{-2}$. They argued that the rapidly decaying bursts are those in which the ejecta was a narrow jet and the break in the light curve was before the first observations. Interestingly, evidence for jets is found when the inferred energy (without taking jets into account) is the largest. This implies that the jets account for a considerable fraction of the wide luminosity distribution seen in GRBs, and the true energy distribution is less wide than it seems to be.

The predicted light-curve transition (from a regular to a fast decay caused by a jet) has been observed in the optical afterglow of GRB 990123 (Kulkarni et al. 1999a; Castro-Tirado et al. 1999; Fruchter et al. 1999). However, no evidence for such an increase in the decay rate was found in near-infrared K-band observations (Kulkarni et al. 1999a). A similar transition was better sampled in afterglow data of GRB 990510; optical observations of GRB 990510, show a clear steepening of the rate of decay of the light simultaneously in all optical bands between ~ 3 hours and several days (Harrison et al. 1999; Stanek et al. 1999) to roughly $F_\nu(t) \propto t^{-2.2}$. Together with radio observations, which also reveal a transition, it is found that the transition is very much frequency-independent; this virtually excludes explanations in terms of the passage of the cooling frequency, but is what is expected in case of beaming (Harrison et al. 1999). Harrison et al. (1999) derive a jet opening angle (from the jet-break time) of $\theta_0 \cong 0.08$, which for this burst would reduce the total energy in γ rays to $\sim 10^{51}$ erg.

Frail et al. (2001) collected the jet-break times for a sample of GRBs with known redshifts. From these, a wide range of jet opening angles is inferred in GRBs: from 3° to more than 25° , with a strong concentration near 4° . This relatively narrow collimation implies that the observed GRB rate has to be corrected for the fact that conical fireballs are visible to only a fraction of observers. Frail et al. find that the 'true' GRB rate is ~ 500 times larger than the observed GRB rate. Although the isotropic equivalent energies of GRBs range from about 5×10^{51} to 1.4×10^{54} erg, when one corrects the observed γ -ray energies for the geometry of the outflow, GRB energies appear narrowly clustered around 5×10^{50} ergs (see Fig. 15.7). Similar conclusions were obtained by Piran et al. (2001) and Panaitescu & Kumar (2001b).

The central engines of GRBs thus produce approximately a similar amount of energy, and the broad range of fluence and luminosity observed for GRBs appears

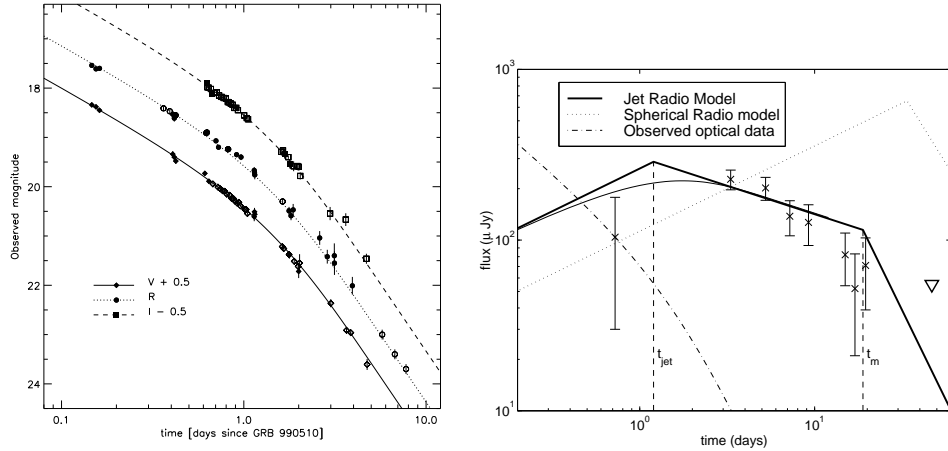


Fig. 15.6. *GRB 990510, the ‘classical’ case for a ‘jet’: an achromatic break in optical and radio at $t_{\text{jet}} = 1.2$ days implying a jet opening angle $\theta_0 = 0.08$. The temporal slope before and after the break agree well with the theory if $p = 2.2$. For this burst the isotropic gamma-ray energy $E_{\text{iso}} = 2.9 \times 10^{53}$ erg but the ‘true’ total energy is only $E = 10^{51}$ erg. From Harrison et al. (1999).*

to be largely the result of a wide variation of opening angles. The reason why this range in angles exists is currently not understood. Our understanding of gamma ray bursts has come a long way in the past four years. It is interesting to note that before the redshift era, most models assumed that the events were standard candles with energies of about 10^{51} erg. As more and more redshifts were determined, the energy record increased steadily up to 10^{54} erg. The standard candle hypothesis was abandoned. It is remarkable that now, when more detailed understanding allows us to infer the beaming angles of these explosions, the true energy budget is back at $\sim 10^{51}$ erg, and the explosions are once again standard candles (though not in the same sense as before).

Postnov, Prokhorov, & Lipunov (2001), Rossi, Lazzati, & Rees.(2002), and Zhang & Mészáros (2002) pointed out that another interpretation is possible for the Frail et. al result. Instead of a variety of jets with different opening angles, a standard jet can be invoked with energy density per unit solid angle falling away from the axis as θ^{-2} ; the differences in the apparent opening angle then come from variations in the orientation of the observer relative to the jet’s axis. Perna, Sari, & Frail (2003) showed that the distribution of the observed opening angles is consistent with this assumption, adding credence to the universal jet model. If this model is correct, the rate of GRBs is much lower, because it should not be corrected by the factor of 500 of Frail et. al.; however, the energy is still low, of order 10^{51} ergs.

15.10 Polarization - A promising tool

An exciting possibility to further constrain the models and obtain a more direct proof of the geometrical picture of ‘jets’ is to measure linear polarization.

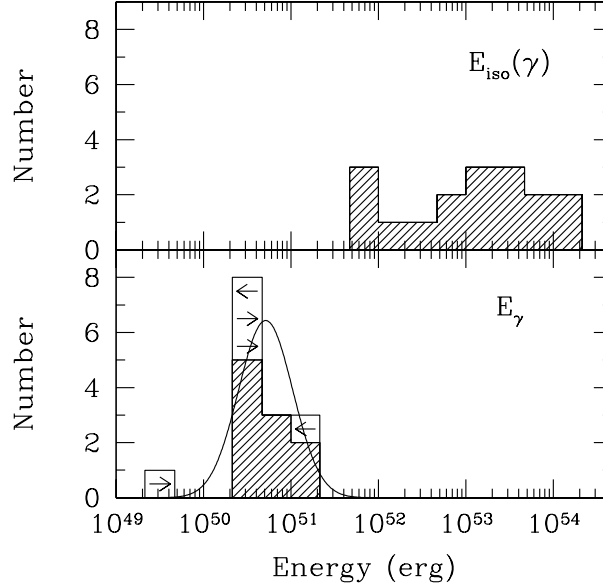


Fig. 15.7. The distribution of the apparent isotropic γ -ray energy of GRBs with known redshifts (top) versus the geometry-corrected energy (bottom). While the isotropic energy E_{iso} spans three orders of magnitudes, the geometrically corrected energy, $E_{\gamma} = E_{\text{iso}}\theta^2/2$, is very narrowly distributed. This implies that the sources of GRBs produce roughly the same amount of energy, about 5×10^{50} erg, but that energy is distributed over a variety of angles resulting in a wide distribution of isotropic energies. From Frail et al. (2001) and Perna et al. (2003).

Varying polarization at optical wavelengths has been observed in GRB afterglows at the level of a few to ten percent (Covino et al. 1999, 2002; Wijers et al. 1999; Rol et al. 2000; Bersier et al. 2003).

High levels of linear polarization are usually the smoking gun of synchrotron radiation. The direction of the polarization is perpendicular to the magnetic field and can be as high as 70%. Gruzinov and Waxman (1999) and Medvedev and Loeb (1999) considered the emission from spherical ejecta which by symmetry should produce no polarization on the average, except for fluctuations of order a few percent. Polarization is more natural if the ejecta are a ‘jet’ and the line of sight to the observer is within the jet but does not coincide with its axis. In this case, the spherical symmetry is broken (Gruzinov 1999; Ghisellini & Lazzati, 1999; Sari 1999), and the polarization produced by synchrotron radiation will not vanish. For simplicity, assume that the magnetic field behind the shock is directed along the shock’s plane (the results hold more generally, as long as the magnetic field has a preferred direction). The synchrotron polarization from each part of the shock front, which is perpendicular to the magnetic field, is therefore directed radially.

As long as the relativistic beaming angle $1/\gamma$ is narrower than the physical size of the jet θ_0 , one is able to see a full ring and therefore the radial polarization averages

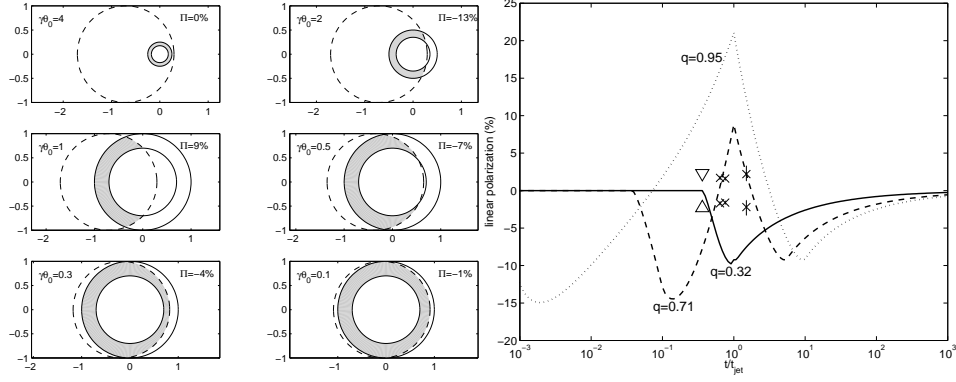


Fig. 15.8. Left: Shape of the emitting region. The dashed line marks the physical extent of the jet, and solid lines give the viewable region $1/\gamma$. The observed radiation arises from the gray shaded region. In each frame, the percentage of polarization is given at the top right and the initial size of the jet relative to $1/\gamma$ is given on the left. The frames are scaled so that the size of the jet is unity. Right: Observed and theoretical polarization lightcurves for three possible offsets of the observer relative to the jet axis. Observational data for GRB 990510 is marked by crosses (x), assuming $t_{jet} = 1.2$ days. The upper limit for GRB 990123 is given by a triangle, assuming $t_{jet} = 2.1$ days.

out (the first frame, with $\gamma\theta_0 = 4$ of the left plot in Figure 15.8). As the flow decelerates, the relativistic beaming angle $1/\gamma$ becomes comparable to θ_0 and only a part of the ring is visible; net polarization is then observed. Note that due to the radial direction of the polarization from each fluid element, the total polarization is maximal when a quarter ($\gamma\theta_0 = 2$ in Figure 15.8) or when three quarters ($\gamma\theta_0 = 1$ in Figure 15.8) of the ring are missing (or radiate less efficiently) and vanishes for a full and a half ring. The polarization, when more than half of the ring is missing, is perpendicular to the polarization direction when less than half of it is missing.

At late stages the jet expands sideways and since the offset of the observer from the physical center of the jet is constant, spherical symmetry is regained. The vanishing and re-occurrence of significant parts of the ring results in a unique prediction: there should be three peaks of polarization, with the polarization position angle during the central peak rotated by 90° with respect to the other two peaks. In case the observer is very close to the center, more than half of the ring is always observed, and therefore only a single direction of polarization is expected. A few possible polarization light curves are presented in Figure 15.8.

15.11 The Reverse Shock Emission: Theory and Observations

The previous sections discussed the theory and the observations of the ‘late’ afterglow, hours or more after the burst. During that time, most of the energy of the system was already given to the shocked surroundings, and it is that region that dominates the emission. However, during the first few tens of seconds, the evolution of the Lorentz factor as a function of time is not self-similar. There are two shocks: a

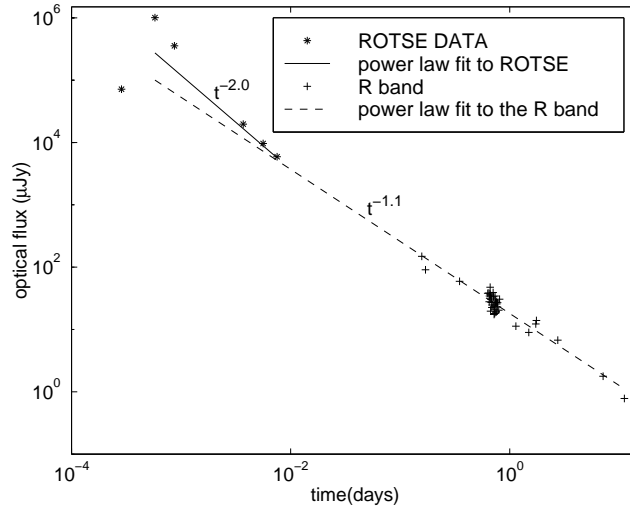


Fig. 15.9. R-band light curve of the afterglow of GRB 990123. The ROTSE data show that the optical light curve peaked at $m_V \sim 9$ (Akerlof et al. 1999). The dashed line indicates a power law fit to the light curve (for $t > 0.1$ days), which has exponent -1.12 ± 0.03 (from Galama et al. 1999).

forward shock going into the surrounding medium and a reverse shock going into the expanding ejecta. The hydrodynamic details were discussed in Sari & Piran (1995).

During the initial stages, the internal energy stored behind the shocked-surrounding matter and the energy of the shocked ejecta are comparable. However, the temperature of the shocked ejecta is much lower, typically by a factor of $\gamma \sim 10^2$. This results in an additional emission component with a typical frequency lower by a factor of $\gamma^2 \sim 10^4$, which, for typical parameters, is near the optical passband. Contrary to the ‘standard’ late afterglow, this emission is very sensitive to the initial Lorentz factor. Theoretical predictions for such a flash were given in detail by Sari & Piran (1999a, 1999c) and were earlier suggested as a possibility by Mészáros & Rees (1997).

One of the most exciting events in the field of afterglow studies was the detection of bright (9th magnitude) optical emission simultaneous with GRB 990123 by the ROTSE team (Akerlof et al. 1999). The ROTSE telescope obtained its first images only 22 seconds after the start of GRB 990123 (i.e. during the GRB), following a notification received from BATSE aboard the Compton Gamma-Ray Observatory. The ROTSE observations show that the optical light curve peaked at $m_V \sim 9$ magnitudes some 60 seconds after the event (Akerlof et al. 1999). After maximum a fast decay followed for at least 15 minutes. The late-time afterglow observations show a more gradual decline (Galama et al. 1999; Kulkarni et al. 1999a; Castro-Tirado et al. 1999; Fruchter et al. 1999, Sari & Piran 1999b) (see Fig. 15.9).

The redshift $z = 1.6$, inferred from absorption features in the OT’s spectrum, implies that the optical flash would have been as bright as the full moon had the GRB occurred in the nearby galaxy M31 (Andromeda). A different way to put

this in perspective is that the flash was some 18 mag brighter (absolute) than the brightest supernovae. Galama et al. (1999) have shown that if one assumes that the emission detected by ROTSE comes from a non-relativistic source of size ct , that then the observed brightness temperature $T_b \geq 10^{17}$ K of the optical flash exceeds the Compton limit of 10^{12} K. This confirms the highly relativistic nature of the GRB source.

The observed optical properties of this event are well described by emission from the reverse shock that initially decelerates the ejecta, provided that the initial Lorentz factor is about 200 (Sari & Piran 1999b; Mészáros & Rees 1999). It takes tens of seconds for the reverse shock to sweep through the ejecta and produce the bright flash. Later, the shocked hot matter expands adiabatically and the emission quickly shifts to lower frequencies and considerably weakens.

The ROTSE observations show that the prompt optical and γ -ray light curves do not track each other (Akerlof et al. 1999). In addition, detailed comparison of the prompt optical emission with the BATSE spectra of GRB 990123 (at three epochs for which both optical and gamma-ray information is available) shows that the ROTSE emission is not a simple extrapolation of the GRB spectrum to much lower energies (Galama et al. 1999; Briggs et al. 1999).

If this interpretation is correct, GRB 990123 would be the first burst in which all three emitting regions have been seen: internal shocks causing the GRB, the reverse shock causing the prompt optical flash, and the forward shock causing the afterglow. The emissions thus arise from three different emitting regions, explaining the lack of correlation between the GRB, the prompt optical and the late-time optical emission (Galama et al. 1999) (but see Liang et al. 1999).

Another new ingredient that was found in GRB 990123 is a radio flare (Kulkarni et al. 1999b). Contrary to all other afterglows, where the radio peaks around a few weeks and then decays slowly, this burst had a fast rising flare, peaking around a day and then decaying quickly. This can be interpreted as emission from the cooling ejecta that was earlier on heated by the reverse shock. Using the Blandford and McKee (1976) self-similar solution to derive the evolution of the ejecta and its emission properties one finds that the typical frequency scales as $\nu_m^r \propto t^{-73/48}$ and the flux at that frequency scales as $F_m^r \propto t^{-47/48}$ (Sari & Piran 1999a) (see Kobayashi & Sari 2001) for revised scalings when the temperature of the ejecta is non-relativistic). Therefore, within a day the emission from the adiabatically cooling ejecta that produced the 60s optical flash in GRB 990123 is expected to shift to radio frequencies (Sari & Piran 1999b). Using the observed optical flash and the above scalings, a good fit to the radio data is obtained. The optical flash and the radio flare may therefore be related.

Given the above interpretation of the reverse shock emission, it is important to ask whether GRB 990123 is an exception, or whether the phenomena of radio flares and optical flashes is more common. Radio flares appear to exist in other cases (Frail et al. 2001). However, since early radio data is usually sparse, and these events did not have an early optical observation to find the associated optical flash, the interpretation in terms of emission from the reverse shock is less secure than in the case of GRB 990123. In the optical, from robotic optical experiments such as ROTSE and LOTIS, strong upper limits exist for several bursts. The upper limits show that

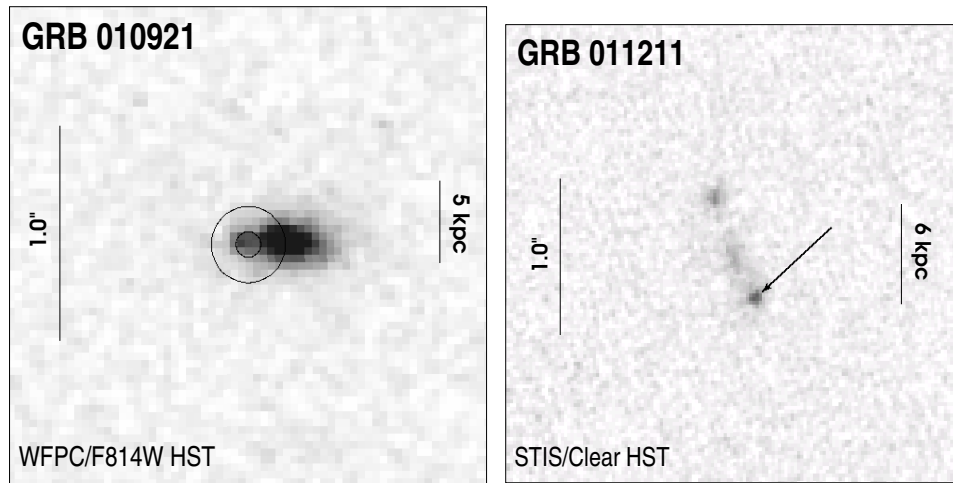


Fig. 15.10. Typical HST images of two GRB host galaxies. The OTs are indicated by the circle (for GRB 010921) and by the arrow (for GRB 011211). Side bars give the projected angular scale, and the physical scale at the source. From Bloom, Kulkarni, & Djorgovski (2002), images courtesy of J.S. Bloom.

the optical flash does not scale with the fluence of the event (Akerlof et al. 2000; Kehoe et al. 2001). However, with reasonably small changes in the density or the initial Lorentz factor, those events could have escaped detection (Kobayashi 2000). HETE-II, or future satellites like Swift, provide or will provide accurate positioning on timescales of seconds, and strong constraints on the generality of optical flashes and radio flares will be obtained.

15.12 GRB Host Galaxies and Redshifts

Host galaxies of GRBs serve a dual purpose: they determine the redshifts, which are necessary for a complete physical modeling of the bursts, and they provide some insights about the possible nature of the progenitors, e.g., their relation to massive star formation, etc. The subject has been reviewed previously, e.g., by Djorgovski et al. (2001b, 2002).

15.12.1 Overall Properties of GRB Hosts

As of this writing (\sim late 2002), plausible or certain host galaxies have been found for all but 1 or 2 of the bursts with optical, radio, or x-ray afterglows localised with arcsecond precision. Two examples are shown in figure 15.10. The median apparent magnitude is $R \approx 25$ mag, with tentative detections or upper limits reaching down to $R \approx 29$ mag. The missing cases are at least qualitatively consistent with being in the faint tail of the observed distribution of host galaxy magnitudes.

Down to $R \sim 25$ mag, the observed distribution is consistent with deep field galaxy counts (Brunner, Connolly, & Szalay 1999), but fainter than that, complex selection effects may be playing a role. It can also be argued that the observed distribution should correspond roughly to luminosity-weighted field galaxy counts. However, the actual distribution would depend on many observational selection and physical

(galaxy evolution) effects, and a full interpretation of the observed distribution of GRB host galaxy magnitudes requires a careful modeling. We note also that the observations in the visible probe the UV in the restframe, and are thus especially susceptible to extinction. However, sub-mm detections of dusty GRB hosts are currently limited by the available technology to only a handful of ultraluminous sources.

Starting with the first redshift measurement which unambiguously demonstrated the cosmological nature of GRBs (Metzger et al. 1997) there are now (late 2002) over 30 redshifts measured for GRB hosts and/or afterglows. The median redshift is $\langle z \rangle \approx 1.0$, spanning the range from 0.25 (or 0.0085, if the association of GRB 980425 with SN 1998bw is correct) to 4.5 (for GRB 000131). The majority of redshifts so far are from the spectroscopy of host galaxies, but an increasing number are based on the absorption-line systems seen in the spectra of the afterglows (which are otherwise featureless power-law continua). Figure 15.11 shows two examples. Reassuring overlap exists in several cases; invariably, the highest- z absorption system corresponds to that of the host galaxy, and has the strongest lines. In some cases (a subset of the so-called “dark bursts”) no optical transient (OT) is detected, but a combination of the X-ray (XT) and radio transient (RT) unambiguously pinpoints the host galaxy.

A new method for obtaining redshifts may come from the X-ray spectroscopy of afterglows, using the Fe K line at ~ 6.55 keV (Piro et al. 1999, 2000; Antonelli et al. 2000), or the Fe absorption edge at ~ 9.28 keV (Weth et al. 2000; Yohshida et al. 1999; Amati et al. 2000). Rapid X-ray spectroscopy of GRB afterglows may become a powerful tool for understanding their physics and origins.

Are the GRB host galaxies special in some way? If GRBs are somehow related to massive star formation (e.g., Paczyński 1998, Totani, 1997, etc.), it may be worthwhile to examine their absolute luminosities and star formation rates (SFR), or spectroscopic properties in general. This is hard to answer (Krumholz, Thorsett, & Harrison 1998; Hogg & Fruchter 1999; Schaefer 2000) from their visible (\sim restframe UV) luminosities alone: the observed light traces an indeterminate mix of recently formed stars and an older population, and cannot be unambiguously interpreted in terms of either the total baryonic mass, or the instantaneous SFR.

The magnitude and redshift distributions of GRB host galaxies are typical for the normal, faint field galaxies, as are their morphologies (Odewahn et al. 1998; Holland 2001; Bloom, Kulkarni & Djorgovski 2002) when observed with the HST: they are often compact, and sometimes suggestive of a merging system (Djorgovski, Bloom & Kulkarni 2001; Hjorth et al. 2002), but that is not unusual for galaxies at comparable redshifts.

Within the host galaxies, the distribution of GRB-host offsets follows the light distribution closely (Bloom, Kulkarni & Djorgovski 2002), which is roughly proportional to the density of star formation (especially for the high- z galaxies). It is thus fully consistent with a progenitor population associated with the sites of massive star formation.

Spectroscopic measurements provide direct estimates of recent, massive SFR in GRB hosts. Most of them are based on the luminosity of the [O II] 3727 doublet (Kennicutt 1998), the luminosity of the UV continuum at $\lambda_{rest} = 2800 \text{ \AA}$ (Madau,

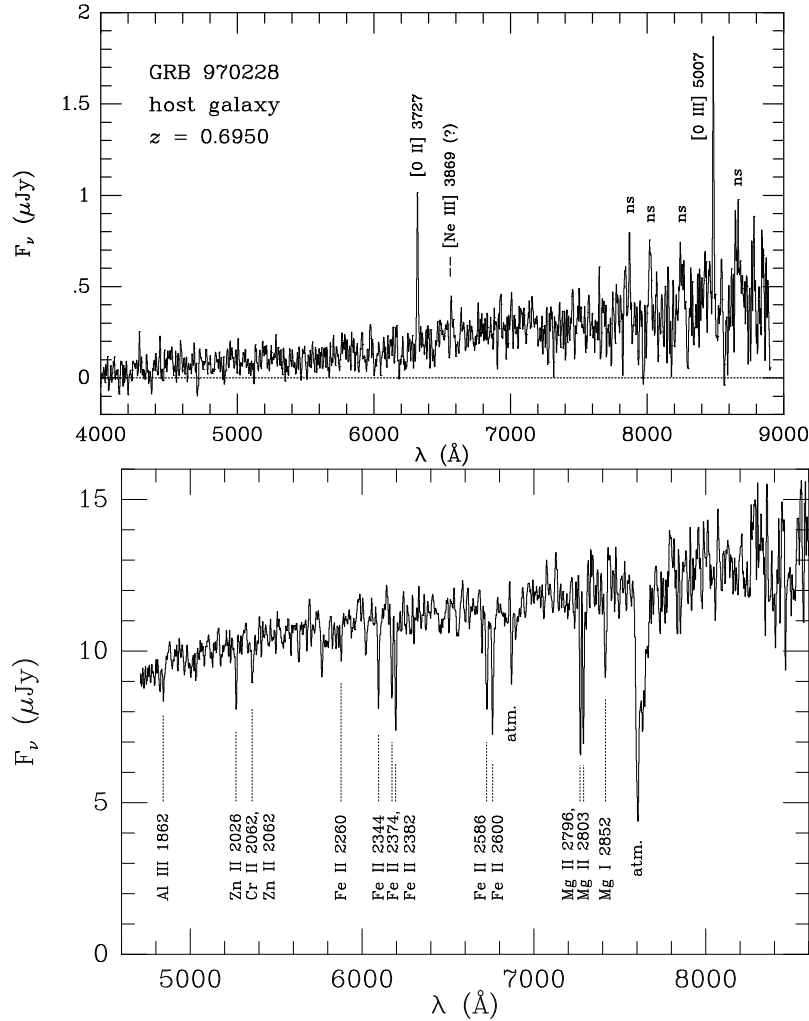


Fig. 15.11. Typical spectra of a GRB host galaxy, showing the standard emission lines indicative of active star formation (for GRB 970228, top), and of an OT, showing the strong absorption lines from the ISM in the host galaxy (for GRB 990123, bottom). The top figure is from Bloom, Djorgovski & Kulkarni (2001). The bottom figure is reprinted by permission from Nature (Kulkarni et al.1999a) copyright 1999 Macmillan Publishers Ltd.

Pozzetti, & Dickinson 1998), in some cases (e.g., Kulkarni et al. 1998) from the luminosity of the Ly α 1216 line, and in others (e.g., Djorgovski et al. 1998) from the luminosity of Balmer lines (Kennicutt 1998). All of these estimators are susceptible to the internal extinction and its geometry, and have an intrinsic scatter of at least 30%. The observed *unobscured* SFR's range from a few tenths to a few $M_\odot \text{ yr}^{-1}$. Applying the reddening corrections derived from the Balmer decrements of the hosts, or from the modeling of the broad-band colors of the OTs (and further assuming that they are representative of the mean extinction for the corresponding host galaxies) increases

these numbers typically by a factor of a few. All this is entirely typical for the normal field galaxy population at comparable redshifts. However, such measurements are completely insensitive to any fully obscured SFR components.

Equivalent widths of the [O II] 3727 doublet in GRB hosts, which may provide a crude measure of the SFR per unit luminosity (and a worse measure of the SFR per unit mass), are on average somewhat higher (Djorgovski et al. 2001a) than those observed in magnitude-limited field galaxy samples at comparable redshifts (Hogg et al. 1998). A larger sample of GRB hosts, and a good comparison sample, matched both in redshift and magnitude range, are necessary before any solid conclusions can be drawn from this apparent difference.

One intriguing hint comes from the flux ratios of [Ne III] 3869 to [O II] 3727 lines: they are on average a factor of 4 to 5 higher in GRB hosts than in star forming galaxies at low redshifts (Djorgovski et al. 2001b). Strong [Ne III] requires photoionization by massive stars in hot H II regions, and may represent indirect evidence linking GRBs with massive star formation.

The interpretation of the luminosities and observed star formation rates is vastly complicated by the unknown amount and geometry of extinction. The observed quantities (in the visible) trace only the unobscured stellar component, or the components seen through optically thin dust. Any stellar and star formation components hidden by optically thick dust cannot be estimated at all from these data, and require radio and sub-mm observations.

Both observational windows, the optical/NIR (rest-frame UV) and the sub-mm (rest-frame FIR) suffer from some biases: the optical band is significantly affected by dust obscuration, while the sub-mm and radio bands lack sensitivity, and therefore uncover only the most prodigiously star-forming galaxies. As of late 2002, radio and/or sub-mm emission powered by obscured star formation has been detected from 4 GRB hosts (Berger, Kulkarni & Frail 2001; Berger et al. 2002b; Frail et al. 2002). The surveys to date are sensitive only to the ultra-luminous ($L > 10^{12}L_{\odot}$) hosts, with SFR of several hundred $M_{\odot} \text{ yr}^{-1}$. Modulo the uncertainties posed by the small number statistics, the surveys indicate that about 20% of GRB hosts are objects of this type, where about 90% of the total star formation takes place in obscured regions.

Given the uncertainties of the geometry of optically thin and optically thick dust, optical colors of GRB hosts cannot be used to make any meaningful statements about their net star formation activity. The broad-band optical colors of GRB hosts are not distinguishable from those of normal field galaxies at comparable magnitudes and redshifts (Bloom, Djorgovski, & Kulkarni 2001; Sokolov et al. 2001). It is notable that the optical/NIR colors of GRB hosts detected in the sub-mm are much bluer than typical sub-mm selected galaxies, suggesting that the GRB selection may be probing a previously unrecognised population of dusty star-forming galaxies.

On the whole, the GRB hosts seem to be representative of the normal, star-forming field galaxy population at comparable redshifts, and so far there is no evidence for any significant systematic differences between them.

15.12.2 GRB Hosts in the Context of Galaxy Evolution

The observed redshift distribution of GRB hosts is about what is expected for an evolving, normal field galaxy population at these magnitude levels. There is an excellent qualitative correspondence between the observations and simple galaxy evolution models (Mao & Mo 1998).

If GRB's follow the luminous mass, then the expected distribution would be approximated by the luminosity-weighted galaxy luminosity function (GLF) for the appropriate redshifts. The hosts span a wide range of luminosities, with a characteristic absolute restframe B band magnitude $M_{B,*} \approx -20$ mag, approximately half a magnitude fainter than in the GLF at $z \approx 0$, but comensurate with the late-type (i.e., star forming disk) galaxy population at $z \approx 0$ (Madgwick et al. 2002; Norberg et al. 2002). This is somewhat surprising, since one expects that the evolutionary effects would make the GRB host galaxies, with a typical $z \sim 1$, brighter than their descendants today. The GRB host GLF also has a somewhat steeper tail than the composite GLF at $z \approx 0$, but again similar to that of the star-forming, late-type galaxies. This is in a broad agreement with the results of deep redshift surveys which probe the evolution of field galaxy populations out to $z \sim 1$ (Lilly et al. 1995; Ellis 1997; Fried et al. 2001; Lin et al. 1999).

The interpretation of these results is complex: the observed light reflects an unknown combination of the unobscured fraction of recent star formation (especially in the high- z galaxies, where we observe the restframe UV continuum) and the stellar populations created up to that point. Our understanding of the field galaxy evolution in the same redshift range as probed by the GRB hosts is still largely incomplete. Different selection effects may be plaguing the field and the GRB host samples. While much remains to be done, it seems that GRB hosts provide a new, independent check on the traditional studies of galaxy evolution at moderate and high redshifts.

15.13 GRBs and Cosmology

While interesting on their own, GRBs are now rapidly becoming powerful tools to study the high-redshift universe and galaxy evolution, thanks to their apparent association with massive star formation, and their brilliant luminosities.

There are three basic ways of learning about the evolution of luminous matter and gas in the universe. First, a direct detection of sources (i.e., galaxies) in emission, either in the UV/optical/NIR (the unobscured components), or in the FIR/sub-mm/radio (the obscured component). Second, the detection of galaxies selected in absorption along the lines of sight to luminous background sources, traditionally QSOs. Third, diffuse extragalactic backgrounds, which bypass all of the flux or surface brightness selection effects plaguing all surveys of discrete sources found in emission, but at a price of losing the redshift information, and the ability to discriminate between the luminosity components powered by star formation and powered by AGN. Studies of GRB hosts and afterglows can contribute to all three of these methodological approaches, bringing in new, independent constraints for models of galaxy evolution and of the history of star formation in the universe.

15.13.1 Dark Bursts: Probing the Obscured Star Formation History

Already within months of the first detections of GRB afterglows, no OT's were found associated with some well-localised bursts despite deep and rapid searches; the prototype “dark burst” was GRB 970828 (Djorgovski et al. 2001a). Perhaps the most likely explanation for the non-detections of OT's when sufficiently deep and prompt searches are made is that they are obscured by dust in their host galaxies. This is an obvious culprit if indeed GRBs are associated with massive star formation.

Support for this idea also comes from detections of RTs without OTs, including GRB 970828, 990506, and possibly also 981226 (see Frail et al. 2000 and Taylor et al. 2000). Dust reddening has been detected directly in some OTs (e.g., Ramakaprash et al. 1998; Bloom et al. 1998; Djorgovski et al. 1998, etc.); however, this only covers OTs seen through optically thin dust, and there must be others, hidden by optically thick dust. An especially dramatic case was the RT (Taylor et al. 1998) and IR transient (Larkin et al. 1998) associated with GRB 980329 (Yost et al. 2002). We thus know that at least some GRB OTs must be obscured by dust.

The census of OT detections for well-localised bursts can thus provide a completely new and independent estimate of the mean obscured star formation fraction in the universe. Recall that GRBs are now detected out to $z \sim 4.5$ and that there is no correlation of the observed fluence with the redshift (Djorgovski et al. 2002), so that they are, at least to a first approximation, good probes of the star formation over the observable universe.

As of late 2002, there have been ~ 70 adequately deep and rapid searches for OTs from well-localised GRBs. We define “adequate searches” as reaching at least to $R \sim 20$ mag within less than a day from the burst, and/or to at least to $R \sim 23 - 24$ mag within 2 or 3 days; this is a purely heuristic, operational definition, and an intentionally liberal one. In just over a half of such searches, OTs were found. Inevitably, some OTs may have been missed due to an intrinsically low flux, an unusually rapid decline rate (Fynbo et al. 2001; Berger et al. 2002a), or very high redshifts (so that the brightness in the commonly used *BVR* bands would be affected by the intergalactic absorption). Thus the *maximum* fraction of all OTs (and therefore massive star formation) hidden by the dust is $\sim 50\%$.

This is a remarkable result. It broadly agrees with the estimates that there is roughly an equal amount of energy in the diffuse optical and FIR backgrounds (see, e.g., Madau 1999). This is contrary to some claims in the literature which suggest that the fraction of the obscured star formation was much higher at high redshifts. Recall also that the fractions of the obscured and unobscured star formation in the local universe are comparable.

There is one possible loophole in this argument: GRBs may be able to destroy the dust in their immediate vicinity (up to ~ 10 pc?) (Waxman & Draine 2000; Galama & Wijers 2000), and if the rest of the optical path through their hosts (\sim kpc scale?) was dust-free, OTs would become visible. Such a geometrical arrangement may be unlikely in most cases, and our argument probably still applies. A more careful treatment of the dust evaporation geometry is needed, but it is probably safe to say that GRBs can provide a valuable new constraint on the history of star formation in the universe.

15.13.2 GRBs as Probes of the ISM in Evolving Galaxies

Absorption spectroscopy of GRB afterglows is now becoming a powerful new probe of the ISM in evolving galaxies, complementary to the traditional studies of QSO absorption line systems. The key point is that the GRBs almost by definition (that is, if they are closely related to the sites of ongoing or recent massive star formation, as the data seem to indicate) probe the lines of sight to dense, central regions of their host galaxies ($\sim 1 - 10$ kpc scale). On the other hand, the QSO absorption systems are selected by the gas cross section, and favor large impact parameters ($\sim 10 - 100$ kpc scale), mostly probing the gaseous halos of field galaxies, where the physical conditions are very different.

The growing body of data on GRB absorption systems shows exceptionally high column densities of gas, when compared to the typical QSO absorption systems; only the highest column density DLA systems (themselves ostensibly star-forming disks or dwarfs) come close (Savaglio, Fall, & Fiore 2002; Castro et al. 2002; Mirabal et al. 2002). This is completely consistent with the general picture described above. (We are referring here to the highest redshift absorbers seen in the afterglow spectra, which are presumably associated with the host galaxies themselves; lower redshift, intervening absorbers are also frequently seen, and their properties appear to be no different from those of the QSO absorbers.)

This opens the interesting prospect of using GRB absorbers as a new probe of the chemical enrichment history in galaxies in a more direct fashion than what is possible with the QSO absorbers, where there may be a very complex dynamics of gas ejection, infall, and mixing at play.

Properties of the GRB absorbers are presumably, but not necessarily (depending on the unknown geometry of the gas along the line of sight) reflecting the ISM of the circum-burst region. Studies of their chemical composition do not yet reveal any clear anomalies, or the degree of depletion of the dust, but the samples in hand are still too small to be really conclusive. Also, there have been a few searches for the variability of the column density of the gas on scales of hours to days after the burst, with no clear detections so far. Such an effect may be expected if the burst afterglow modifies the physical state of the gas and dust along the line of sight by the evaporation of the dust grains, additional photoionization of the gas, etc. However, it is possible that all such changes are observable only on very short time scales, seconds to minutes after the burst. In any case, a clear detection of a variable ISM absorption against a GRB afterglow would be a very significant result, providing new insight into the circumstances of GRB origins.

15.13.3 High-Redshift GRBs: Probing the Primordial Star Formation and Reionization

Possibly the most interesting use of GRBs in cosmology is as probes of the early phases of star and galaxy formation, and the resulting reionization of the universe at $z \sim 6 - 20$. If GRBs reflect deaths of massive stars, their very existence and statistics would provide a superb probe of the primordial massive star formation and the initial mass function (IMF). They would be by far the most luminous sources in existence at such redshifts (much brighter than SNe, and most AGN), and they may exist at redshifts where there were *no* luminous AGN. As such, they would

provide unique new insights into the physics and evolution of the primordial IGM during the reionization era (see, e.g., Lamb & Reichart 2001; Loeb 2002a,b).

There are two lines of argument in support of the existence of copious numbers of GRBs at $z > 5$ or even 10. First, a number of studies using photometric redshift indicators for GRBs suggests that a substantial fraction (ranging from $\sim 10\%$ to $\sim 50\%$) of all bursts detectable by past, current, or forthcoming missions may be originating at such high redshifts, even after folding in the appropriate spacecraft/instrument selection functions (Fenimore & Ramirez-Ruiz 2002; Reichart et al. 2001; Lloyd-Ronning, Fryer, & Ramirez-Ruiz 2002).

Second, a number of modern theoretical studies suggest that the very first generation of stars, formed through hydrogen cooling alone, were very massive, with $M \sim 100 - 1000 M_{\odot}$ (Bromm, Coppi & Larson 1999; Abel, Bryan, & Norman 2000; Bromm, Kudritzki, & Loeb 2001; Bromm, Coppi & Larson 2002; Abel, Bryan & Norman 2002). While it is not yet absolutely clear that some as-yet unforeseen effect would lead to a substantial fragmentation of a protostellar object of such a mass, a top-heavy primordial IMF is at least plausible. It is also not yet completely clear that the (probably spectacular) end of such an object would generate a GRB, but that too is at least plausible (Fryer, Woosley & Heger 2001). Thus, there is some real hope that significant numbers of GRBs and their afterglows would be detectable in the redshift range $z \sim 5 - 20$, spanning the era of the first star formation and cosmic reionization (Bromm & Loeb 2002).

Spectroscopy of GRB afterglows at such redshifts would provide a crucial, unique information about the physical state and evolution of the primordial ISM during the reionization era. The end stages of the cosmic reionization have been detected by spectroscopy of QSOs at $z \sim 6$ (Djorgovski et al. 2001c; Fan et al. 2001; Becker et al. 2001). GRBs are more useful in this context than the QSOs, for several reasons. First, they may exist at high redshifts where there were no comparably luminous AGN yet. Second, their spectra are highly predictable power-laws, without complications caused by the broad Ly α lines of QSOs, and can reliably be extrapolated blueward of the Ly α line. Finally, they would provide a genuine snapshot of the intervening ISM, without an appreciable proximity effect which would inevitably complicate the interpretation of any high- z QSO spectrum (luminous QSOs excavate their Stromgren spheres in the surrounding neutral ISM out to radii of at least a few Mpc, whereas the primordial GRB hosts would have a negligible effect of that type; see, e.g., Lazzati et al.(2001).

Detection of high- z GRBs is thus an urgent cosmological task. It requires a rapid search for afterglows, as well as high-resolution follow-up spectroscopy, in both the optical and NIR. However, such effort would be well worth the considerable scientific rewards in the end.

15.14 Acknowledgments

SGD and RS wish to thank numerous collaborators, including S.R. Kulkarni, D.A. Frail, F.A. Harrison, J.S. Bloom, T. Galama, D. Reichart, D. Fox, E. Berger, P. Price, S. Yost, A. Soderberg, S.M. Castro, A. Mahabal, R. Goodrich, F. Chaffee, J. Halpern, and many others. Our work was supported by grants from the NSF, NASA, and private donors.

References

- Abel, T., Bryan, G., & Norman, M. 2000, ApJ 540, 39
Abel, T., Bryan, G., & Norman, M. 2002, Science 295, 93
Akerlof, C., et al. 1999, Nature 398, 400
Akerlof, C., et al. 2000, ApJL 532, L25
Amati, L., et al. 2000, Science 290, 953
Andersen, M., et al. 2000, A&A. 364, L54
Antonelli, L.A., et al. 2000, ApJ 545, L39
Atkins, R., et al. 2000, ApJ 533, L119
Band, D., et al. 1993, ApJ 413, 281
S. D. Barthelmy, T. L. Cline, & P. Butterworth 2001, in Gamma Ray Bursts, ed. R. M. Kippen, R. S. Mallozzi, & G. J. Fishman (AIP press, New York)
Baring, M. G. & Harding, A. K. 1997, ApJ 491, 663
Becker, R., et al. (the SDSS collaboration) 2001, AJ 122, 2850
Beloboradov, A. 2000, ApJ 539, 25
Berger, E., et al. 2000, ApJ 545, 56
Berger, E., Kulkarni, S.R., & Frail, D.A. 2001, ApJ, 560, 652
Berger, E., et al. 2002a, submitted to ApJ [astro-ph/0207320]
Berger, E., et al. 2002b, submitted to ApJ [astro-ph/0210645]
Bersier, D., et al. 2003, ApJ 583, L63
Bhat, P., et al. 1994, ApJ 426, 604
Blandford, R. & Mc Kee, C.F. 1976, Phys. Fluids 19, 1130
Blandford, R. & Znajek, R. 1977, MNRAS 179, 433
Bloom, J.S., et al. 1998, ApJ 508, L21
Bloom, J., et al. 1999, Nature 401, 453
Bloom, J.S., Djorgovski, S.G. & Kulkarni, S.R. 2001, ApJ 554, 678
Bloom, J.S., Kulkarni, S.R., & Djorgovski, S.G. 2002, AJ 123, 1111
Bremer, M., et al. 1998, A&A 332, L13
Briggs, M.S., et al. 1999, ApJ 524, 82
Bromm, V., Coppi, P., & Larson, R. 1999, ApJ 527, L5
Bromm, V., Coppi, P., & Larson, R. 2002, ApJ 564, 23
Bromm, V., Kudritzki, R., & Loeb, A. 2001, ApJ 552, 464
Bromm, V., & Loeb, A. 2002, ApJ 575, 111
Bromm, V., & Schaefer, B. 1999, ApJ 520, 661
Brunner, R., Connolly, A., & Szalay, A. 1999, ApJ 516, 563
Burenin, R., et al. 1999, A&A. 344, L53
Castro, S., et al. 2002, ApJ, in press
Castro-Tirado, A., et al. 1998, Science 279, 1011
Castro-Tirado, A., et al. 1999, Science 283, 2069
Chevalier, R.A. & Li, Z. 1999, ApJL 520, L29
Cohen, E., Piran T. & Sari, R. 1998, ApJ 509, 717
Costa, E., et al. 1997, Nature 387, 783
Costa, E. 2000, in Gamma-Ray Bursts, ed. R. M. Kippen, R. S. Mallozzi, & G. J. Fishman (AIP press, New York)
Costa, E., Frontera, F., & Hjorth, J. 2001 "Gamma-Ray Bursts in the Afterglow Era", Berlin: Springer Verlag
Covino, S., et al. 1999, A & A 348, L1
Covino, S., et al. 2002, A & A 392, 865
Dar, A., & De Rujula, A. 2
Dermer, C., & Mitman, K. 1999, ApJ 513, L5
Dezalay, J.-P., et al. 1996, ApJ 471, L27
Djorgovski, S.G., et al. 1998, ApJ 508, L17
Djorgovski, S.G., et al. 2001a, ApJ 562, 654
Djorgovski, S.G., et al. 2001b, in Gamma-Ray Bursts in the Afterglow Era: 2nd Workshop, eds. E. Costa et al., ESO Astrophysics Symposia, Berlin: Springer Verlag, p. 218

36 *Gamma-ray bursts*

- Djorgovski, S.G., et al. 2001c, ApJ 560, L5
Djorgovski, S.G., Bloom, J.S., & Kulkarni, S.R. 2002, ApJ in press [astro-ph/0008029]
Djorgovski, S.G., et al. 2002, in Proc. IX Marcel Grossmann Meeting, eds. V. Gurzadyan et al. Singapore: World Scientific, in press [astro-ph/0106574]
Eichler, D., et al. 1989, Nature 340, 126
Ellis, R. 1997, ARAA 35, 389
Fan, X., et al. (the SDSS collaboration) 2001, AJ 122, 2833
Fenimore, E. E., Epstein, R. I., & Ho, C. 1993, A&AS 97, 59
Fenimore, E. E., Madras, C. D. & Nayakchin, S. 1996, ApJ 473, 998
Fenimore, E., & Ramirez-Ruiz, E. 2002, ApJ, in press [astro-ph/0004176]
Fox, D., et al. 2002, GCN GRB Observation Report 1569
Frail, D.A., et al. 1994, ApJ 437, L43
Frail, D.A., et al. 1997, Nature 389, 261
Frail, D.A., et al. 2000, ApJ 538, L129
Frail, D.A., et al. 2001, ApJ 562, L55
Frail, D.A., Waxman, E. & Kulkarni, S.R. 2000, ApJ 537, 191
Frail, D.A., et al. 2001, ApJ 562, L55
Frail, D.A., et al. 2002, ApJ 565, 829
Fried, J., et al. 2001, A&A 367, 788
Frontera, F., et al. 2000, ApJS 127, 59
Fruchter, A., et al. 1999, ApJL 519, L13
Fruchter, A., et al. 2000, ApJ 545, 664
Fryer, C., Woosley, S., & Heger, A. 2001, ApJ 550, 372
Fynbo, J., et al. 2001, A&A 369, 373
Galama, T.J., et al. 1997a, A&A 321, 229
Galama, T.J., et al. 1997b, Nature 387, 479
Galama, T.J., et al. 1998a, ApJL 497, L13
Galama, T.J., et al. 1998b, ApJL 501, L97
Galama, T.J., et al. 1998c, Nature 395, 670
Galama, T.J., et al. 1999, Nature 398, 394
Galama, T.J., & Wijers, R. 2000, ApJ 549, L209
Galama, T.J., et al. 2001, in preparation
Goodman, J. 1986, ApJL 308, 46
Granot, J., Piran, T. & Sari, R. 1999, ApJL 527, 236
Granot, J., Piran, T. & Sari, R. 2000a, ApJ 513, 679
Granot, J., Piran, T. & Sari, R. 2000b, ApJ 534, L163
Ghisellini, G., & Lazzati, D. 1999, MNRAS 309, L7
Gruzinov A. 1999, ApJ 525, L29
Gruzinov A., & Waxman E., 1999, ApJ 511, 852
Harris, M., & Share, G. 1998, ApJ 494, 724
Harrison, F.A., et al. 1999, ApJL 523, L121
Harrison, F.A., et al. 2001, ApJ 559, 123
Heise, J., et al. 2001, in Gamma-Ray Bursts in the Afterglow Era, ed. E. Costa, F. Frontera, & J. Hjorth (Springer - Berlin)
Hjorth, J., et al. 2002, ApJ 576, 113
Holland, S. 2001, [astro-ph/0102413]
Hogg, D., et al. 1998, ApJ 504, 622
Hogg, D., & Fruchter, A. 1999, ApJ 520, 54
Hurley, K. 1992, in Gamma-Ray Bursts ed. W. Paciesas & G. Fishman (AIP Press- New York)
Hurley, K., et al. 1994, Nature 372, 652
Hurley, K., et al. 2000, ApJ 534, L23
Hurley, K., et al. 2002, ApJ 567, 447
Jager, R., et al. 1993, Adv. Space Res. 13, 12, 315
Katz, J. I. 1994, ApJ 422, 248
Katz, J. I. 2002, The Biggest Bangs (Oxford University Press, New York)
Kehoe, R., et al. 2001, ApJ 554, L159
Kennicut, R. 1998, ARAA 36, 131

- Kippen, R., et al. 2001, in *Gamma-Ray Bursts in the Afterglow Era*, ed. E. Costa, F. Frontera, & J. Hjorth (Springer - Berlin)
- Kobayashi, S. 2000, *ApJ* 545, 807
- Kobayashi, S., Piran, T., & Sari, R. 1997, *ApJ* 490, 92
- Kobayashi, S. & Sari, R. 2001, *ApJ* 551, 934
- Kommers, J., et al. 2000, *ApJ* 533, 696
- Koranyi, D.M., et al. 1995 *MNRAS* 276, L13
- Kouveliotou, C., et al. 1993, *ApJ* 413, L101
- Krolik, J. H. & Pier, E. A. 1991, *ApJ* 373, 277
- Krumholtz, M., Thorsett, S., & Harrison, F. 1998, *ApJ* 506, L81
- Kulkarni, S.R., et al. 1998, *Nature* 393, 35
- Kulkarni, S.R., et al. 1999a, *Nature* 398, 389
- Kulkarni, S. R., et al. 1999b, *ApJ* 522, L97
- Kumar, P., & Piran, T. 2000, *ApJ* 532, 286
- Lamb, D., & Reichart, D. 2000, *ApJ* 536, 1
- Lamb, D., & Reichart, D. 2001, in *Gamma-Ray Bursts in the Afterglow Era: 2nd Workshop*, eds. E. Costa et al., *ESO Astrophysics Symposia*, Berlin: Springer Verlag, p. 226
- Larkin, J., et al. 1998, *GCN Circ.* 44
- Lazzati, D., et al. 2001, in *Gamma-Ray Bursts in the Afterglow Era: 2nd Workshop*, eds. E. Costa et al., *ESO Astrophysics Symposia*, Berlin: Springer Verlag, p. 236
- Li, L. & Paczyński, B. 1998, *ApJL* 507, L59
- Liang, E.P., et al. 1999, *ApJL* 519, L21
- Lilly, S., et al. 1995, *ApJ* 455, 108
- Lin, H., et al. 1999, *ApJ* 518, 533
- Lithwick, Y., & Sari, R. 2001, *ApJ* 555, 540
- Lloyd-Ronning, N., Fryer, C., & Ramirez-Ruiz, E. 2002, *ApJ* 574, 554
- Loeb, A. 2002a, in *Lighthouses of the Universe: The Most Luminous Celestial Objects and Their Use for Cosmology*, Eds. M. Gilfanov, R. Sunyaev & E. Churazov, Berlin: Springer Verlag, p. 137
- Loeb, A. 2002b, in *Supernovae and Gamma-Ray Bursters*, ed. K. Weiler, Berlin: Springer Verlag, in press [astro-ph/0106455]
- MacFadyen, A., & Woosley, S. 1999a, *ApJ* 524, 262
- MacFadyen, A. & Woosley, S. 1999b, *ApJ* 526, 152
- Madau, P., Pozzetti, L., & Dickinson, M. 1998, *ApJ* 498, 106
- Madau, P. 1999, *ASPCS* 193, 475
- Madgwick, D., et al. (the 2dF team) 2002, *MNRAS* 333, 133
- Mallozzi, R., et al. 1995, *ApJ* 454, 597
- Mao, S. & Yi, I. 1994, *ApJ* 424, L131
- Mao, S., & Mo, H.J. 1998, *A&A* 339, L1
- Mazets, E., et al. 1981a, *Ap&SS* 80, 3
- Mazets, E., et al. 1981b, *Ap&SS* 80, 119
- McBreen, B., et al. 1994, *MNRAS* 271, 662
- McNamara, B.E., et al. 1995, *Ap&SS* 231, 251
- Medvedev, M. V., & Loeb A. 1999, *ApJ* 526, 697
- Mészáros, P. & Rees, M. J. 1993, *ApJ* 405, 278
- Mészáros, P., & Rees M. J. 1999, *MNRAS* 299, L10
- Mészáros, P., & Rees M. J. 1997, *ApJ* 476, 232
- Mészáros, P. & Rees, M. J. 1999, *MNRAS* 306, L39
- Mszros, P. Rees, M. & Wijers, R.A.M.J. 1998, *ApJ* 499, 301
- Metzger, M.R., et al. 1997, *Nature* 387, 879
- Mochkovitch, R., et al. 1993, *Nature* 361, 236
- Moderski, R., Sikora, M., Bulik, T. 2000, *ApJ* 529, 151
- Mirabal, M., et al. 2002, *ApJ* 578, 818
- Nakar, E., & Piran, T. 2002, *MNRAS* 331, 40
- Narayan, R. & Paczyński, B. & Piran, T. 1992, *ApJL* 395, L83
- Norberg, P., et al. (the 2dF team) 2002, *MNRAS*, 336, 907
- Norris, J., et al. 1984, *Nature* 308, 434

- Odehahn, S.C., et al. 1998, ApJ 509, L5
Paciesas, W., et al. 1999, ApJS 122, 465
Paczynski, B. 1986, ApJ 308, L43
Paczynski, B. 1993, Ann. NY Acad Sci. 688, 321
Paczynski, B. & Rhoads, J. 1993, ApJ 418, L5
Paczynski, B. 1998, ApJ 494, L45
Panaitescu, A. 2001, ApJ 556, 1002
Panaitescu, A. & Kumar, P. 2001a, ApJ 554, 667
Panaitescu, A., and Kumar, P. 2001b, ApJ 560, L49
Panaitescu A., Mészáros, P. 1998, ApJL 493, L31
Panaitescu, A. & Mészáros, P. 1999, ApJ 503, 314
Pendleton, G., et al. 1996, ApJ 464, 606
Perna, R., Sari, R. & Frail, D.A. 2003, submitted to apJ.
Piran, T., & Shemi, A. 1993, ApJ 403, L67
Piran, T., Shemi, A., & Narayan, R. 1993, MNRAS 263, 861
Piran, T. 1999, in Gamma Ray Bursts: The First Three Minutes', Ed. Juri Poutanen, ASP Conf. Ser. 190, 3 (Astronomical Society of the Pacific, San Francisco, CA, USA)
Piran, T., et al. 2001, ApJ 560, L167
Piro, L., Scarsi, L. & Butler, R.C. 1995, Proc. SPIE 2517, 169
Piro, L., et al. 1998, A&A 331, L41
Piro, L., et al. 1999, A&ASup 138, 431
Piro, L., et al. 2000, Science 290, 955
Postnov, K. A., Prokhorov, M. E., & Lipunov, V. M. 2001, Astronomy Reports 45, 236
Ramaprakash, A., et al. 1998, Nature 393, 43
Ramirez-Ruiz, E., & Fenimore, E. E. 1999, A&A 138, 521
Rees, M. J. & Mészáros, P. 1994, ApJL 403, L93
Reichart, D.E. 1997, ApJL 485, L57
Reichart, D., et al. 2001, ApJ 552, 57
Rhoads, J.E. 1997, ApJL 478, L1
Rhoads, J. E. 1999, ApJ 525, 737
Rol, E., et al. 2000, ApJ 544, 707
Rossi, E., Lazzati, D. & Rees, M. J. 2002, MNRAS 332, 945
Sahu, K.C. et al. 1997, Nature 387, 476
Sari, R. 1997, ApJL 489, L37
Sari, R. 1998, ApJL 494, L17
Sari, R. 1999, ApJ 524, L43
Sari, R. & Esin A. 2001, ApJ 548, 787
Sari, R., & Mészáros, P. 2000, ApJ 535, L33
Sari, R., Narayan, R. & Piran, T. 1996, ApJ 473, 204
Sari, R., & Piran T. 1995, ApJ 455, L143
Sari, R., & Piran T. 1997a, ApJ 485, 270
Sari, R., & Piran T. 1997b, MNRAS 287, 110
Sari, R. & Piran, T. 1999a, ApJ 520, 641
Sari, R. & Piran, T. 1999b, ApJL 517, L109
Sari, R., & Piran, T. 1999c, A&A 138, 537.
Sari, R., Piran, T. & Halpern, J. 1999, ApJ 519, L17
Sari, R., Piran, T. & Narayan, R. 1998, ApJL 497, L17
Savaglio, S., Fall, S.M., & Fiore, F. 2002, ApJ, in press
Schaefer, B. 2000, ApJ 532, L21
Schilling, G. 2002, Flash! The Hunt for the Biggest Explosions in the Universe (Cambridge University Press, Cambridge).
Schmidt, M. 1999, ApJ 523, L117
Schmidt, M. 2001, ApJ 552, 36
Sokolov, V.V., et al. 2001, A&A 372, 428
Stanek, K.Z., et al. 1999, ApJL 522, L39
Stern, B., et al. 2001, ApJ 563, 80
Stern, B., Atteia, J.-L., & Hurley, K. 2002, ApJ 304, 304

15.14 Acknowledgments

39

- Taylor, G.B., et al. 1998, ApJ 502, L115
Taylor, G.B., et al. 2000, ApJ 537, L17
Totani, T. 1997, ApJ 486, L71
van Paradijs, J., et al. 1997, Nature 386, 686
Vietri, M. 1997, ApJ 478, L9
Waxman, E. 1997, ApJL 485, L5
Waxman, E. 1997, ApJL 491, L19
Waxman, E., & Draine, B. 2000, ApJ 537, 796
Weth, C., et al. 2000, ApJ 534, 581
Wijers, R.A.M.J., Rees, M.J. & Mészáros, P. 1997, MNRAS 288, L51
Wijers, R.A.M.J., et al. 1999, ApJL 523, L33
Wijers, R.A.M.J. & Galama, T.J 1999, ApJ 523, 177
Yoshida, A., et al. 1999, A&ASup 138, 433
Yost, S., et al. 2002, ApJ 577, 155
Zhang, B. & Mészáros, P. 2002, ApJ 571, 876

